Geological Magazine

www.cambridge.org/geo

The Late Cretaceous metamorphic rocks of the Akrotiri and Vari subunits on Tinos and Syros, Cyclades, Greece: field observations, geochemistry and geochronology

Michael Bröcker and Jasper Berndt

Institut für Mineralogie, Universität Münster, Münster, Germany

Original Article

Cite this article: Bröcker M and Berndt J. The Late Cretaceous metamorphic rocks of the Akrotiri and Vari subunits on Tinos and Syros, Cyclades, Greece: field observations, geochemistry and geochronology. *Geological Magazine* https://doi.org/10.1017/S0016756824000219

Received: 16 April 2024
Revised: 1 August 2024
Accepted: 12 August 2024

Keywords:
Akrotiri subunit; Vari subunit; Asterousia nappe; Riebeckite; U–Pb geochronology

Corresponding author:
Michael Bröcker; Email: michael.broecker@uni-muenster.de

Abstract

The relationship of the Late Cretaceous amphibolite-facies Akrotiri and Vari subunits on the Greek islands of Tinos and Syros to similar occurrences in the Aegean is not fully understood, but a correlation with the Asterousia Crystalline Complex on Crete and corresponding rocks in the Upper Cycladic Unit on other islands of the archipelago is a plausible interpretation. There is currently no clear evidence that the Akrotiri subunit represents a fragment of the metamorphic sole of the nearby Tsiknias ophiolite, as there are differences in field appearance, geochemistry, metamorphic grade and retrograde overprint. Felsic rocks from amphibolite-gneiss sequences of the Akrotiri and Vari subunits are interpreted as reworked igneous rocks with minor admixture of terrigenous material. The Triassic U–Pb zircon age (*c.* 240 Ma) of such a gneiss from Syros indicates the magmatic crystallization age of the original source rocks. A similar interpretation is suggested for the studied Akrotiri gneiss, but is less clear due to the not fully clarified significance of the presumed Pb loss thought to be responsible for the considerable U–Pb age range of the dated zircons (*c.* 256–114 Ma). The Vari gneiss sensu strictu is closely associated with metadioritic rocks containing a Triassic zircon population (*c.* 238 Ma). The protolith is probably plutonic, but a mixture of volcanic and plutonic detritus cannot be excluded. Riebeckitic amphiboles occur in all rock types of the Akrotiri subunit, indicating late overprinting at elevated pressures, which is not known from similar occurrences in the southern Aegean.

1. Introduction

From Crete and many Aegean islands (e.g. Anafi, Dounoussa, Ikaria, Nikouria, Tinos; Fig. 1a), Late Cretaceous amphibolite-facies rocks and associated (meta)granitoids have been reported (e.g. Dürr *et al.* 1978a, b; Seidel *et al.* 1976, 1981; Reinecke *et al.* 1982; Dürr, 1986; Altherr *et al.* 1994; Patzak *et al.* 1994; Be´eri-Shlevin *et al.* 2009; Kneuker *et al.* 2015; Martha *et al.* 2016, 2017, 2019). These occurrences are generally interpreted as remnants of rock sequences from the hanging wall of a Mesozoic-Cenozoic subduction system that remained unaffected by high-pressure/low-temperature metamorphism (e.g. Dürr *et al.* 1978a; Be´eri-Shlevin *et al.* 2009; Martha *et al.* 2016).

The focus of this study is on the Akrotiri and Vari subunits on the Cycladic islands of Tinos and Syros (Fig. 1), which share many features with other occurrences of Late Cretaceous amphibolite-facies rocks in the greater region (Bröcker & Enders, 2001; Soukis & Stockli, 2013). However, their status within the overall structure of the Aegean has not yet been fully clarified. Both subunits either belong to a specific tectonic subunit above the Cycladic Blueschist Unit, e.g. the Asterousia nappe, or are associated with the metamorphic sole of the Tsiknias ophiolite, the closest occurrence of amphibolite-facies rocks in the immediate vicinity (Patzak *et al.* 1994; Katzir *et al.* 1996; Lamont *et al.* 2020a). Taking into account previous work and new observations and data, we describe the field conditions, petrographic, mineralogical, geochemical and geochronological features and try to decipher possible correlative relationships in the local and regional context.

2. Geological setting

2.a. The Attic-Cycladic Crystalline Belt

The geology, petrology and tectonics of the larger study area have been the subject of detailed studies for decades. Only a summary of the most important features is given here.

The Attic-Cycladic Crystalline Belt (Fig. 1a) consists of two major tectonic units with different pressure-temperature-deformation-time (*P–T–D–t*) histories, both of which comprise numerous fault-bounded subunits (e.g. Dürr *et al.* 1978a; Forster and Lister 2005; Ring *et al.* 2010). The

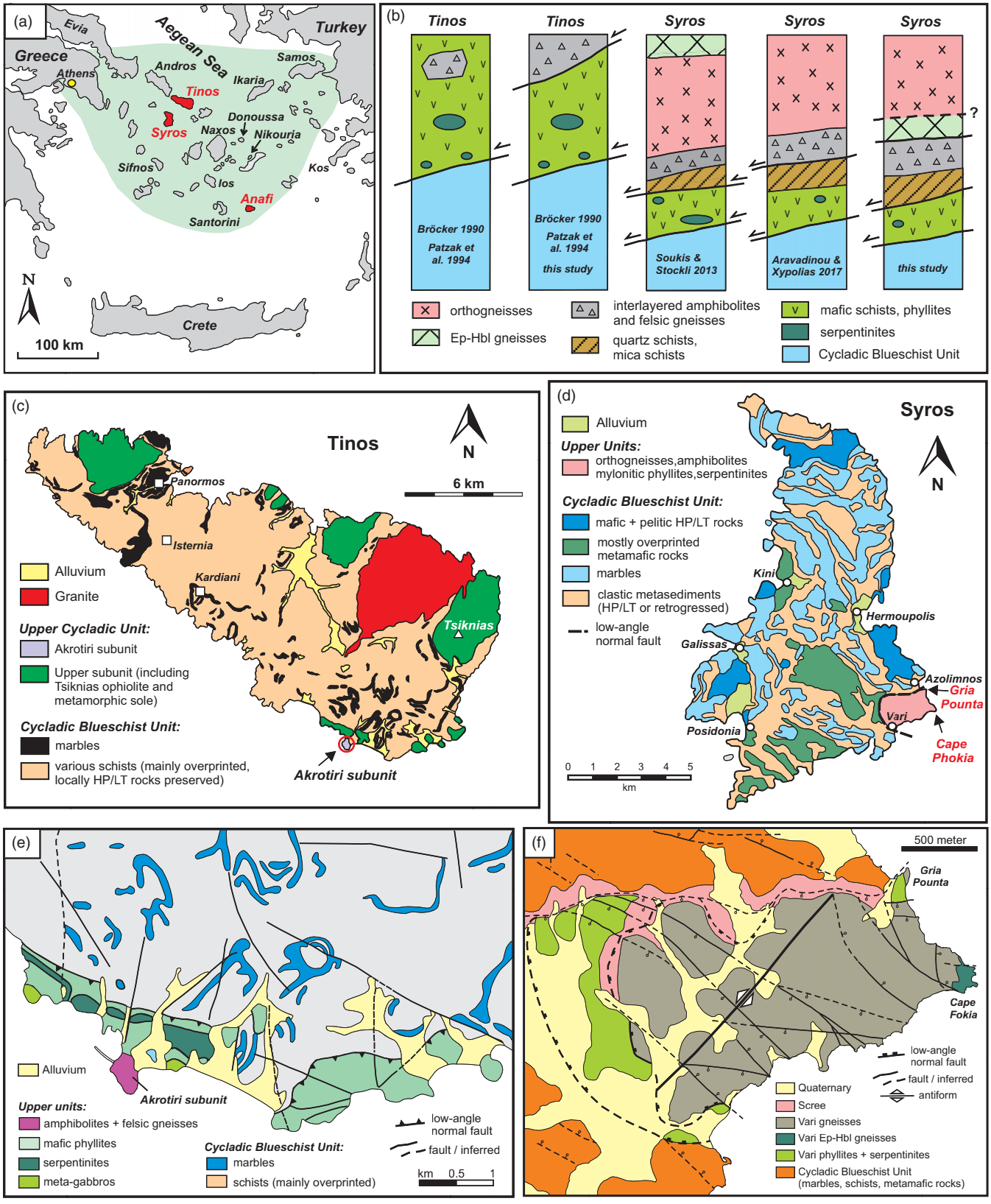

Figure 1. (Colour online) (a) Geographic overview map of the larger study area showing in green the regional distribution of the Attic–Cycladic Crystalline Belt. (b) Schematic tectono-stratigraphic columns (not to scale) showing different interpretations for the uppermost part of the metamorphic nappe stack on Tinos and Syros. (c, d) Simplified geological maps of Tinos (modified after Melidonis, 1980) and Syros (modified after Keiter *et al.* 2004, 2011). (e) Close-up geological maps of the area around the Akrotiri subunit (simplified after IGME 2003) and of (f) SE Syros (modified after Soukis & Stockli, 2013). (This and all other figures are published in colour online).

https://doi.org/10.1017/S0016756824000219 Published online by Cambridge University Press

Upper Cycladic Unit includes a heterogeneous sequence of unmetamorphosed Permian to Miocene sediments, Jurassic and undated ophiolitic and metamorphic sole remnants, greenschist-facies rocks with Cretaceous to Palaeogene metamorphic ages as well as Late Cretaceous amphibolite-facies rocks and (meta)granitoids (e.g. Altherr *et al.* 1994; Patzak *et al.* 1994; Sanchez-Gomez *et al.* 2002; Kuhlemann *et al.* 2004; Be´eri-Shlevin *et al.* 2009; Martha *et al.* 2016; Lamont *et al.* 2020a). Evidence for high-pressure/low-temperature (HP/LT) metamorphism, a key feature in the metamorphic evolution of the structurally lower Cycladic Blueschist Unit, was not recognized in any of these parts. The group of upper units was juxtaposed by low-angle detachments onto the Cycladic Blueschist Unit (Avigad & Garfunkel, 1989; Brichau *et al.* 2007; Jolivet & Brun, 2010; Jolivet *et al.* 2010), which also consists of several tectonic subunits that can be assigned to an upper and lower group of blueschist-facies nappes (Grasemann *et al.* 2018; Glodny & Ring, 2022). The lower group was affected by peak conditions of 400 ± 20°C and 1.0 ± 0.2 GPa, whereas the upper group records temperatures and pressures of 550 ± 50°C and 2.0 ± 0.2 GPa, respectively (Grasemann *et al.* 2018). Between *c.* 55 Ma and *c.* 15 Ma, the Cycladic Blueschist Unit was affected by eclogite- to epidote-blueschist-facies metamorphism and subsequent overprinting at lower pressure blueschist-, greenschist-, or amphibolite-facies *P–T* conditions (e.g. Altherr *et al.* 1979; Okrusch & Bröcker, 1990; Wijbrans *et al.* 1990; Bröcker *et al.* 1993, 2004, 2013; Tomaschek *et al.* 2003; Lagos *et al.* 2007; Ring *et al.* 2010; Putlitz *et al.* 2005; Cliff *et al.* 2017; Peillod *et al.* 2017; Laurent *et al.* 2016, 2017, 2021; Lamont *et al.* 2020b; Glodny & Ring, 2022, and references therein).

2.b. The Akrotiri and Upper subunits of Tinos

The metamorphic succession of Tinos Island is traditionally divided into at least three tectonic subunits (Fig. 1b, c). The Akrotiri and Upper subunits, which form the uppermost part of the metamorphic sequence, belong to the regional Upper Cycladic Unit and record amphibolite and greenschist-facies *P–T* conditions (e.g. Melidonis, 1980; Patzak *et al.* 1994; Katzir *et al.* 1996; Bröcker & Franz, 1998; Zeffren *et al.* 2005; Lamont *et al.* 2020a). The Lower subunit (~1250-1800 m thick) is part of the Cycladic Blueschist Unit and therefore not relevant to the questions discussed here. For details, see Lamont *et al.* (2020b, and references therein). The following description focuses on the structurally higher rock series.

The Akrotiri subunit (300–350m thick) is exposed in a relatively small outcrop near the main village (Fig. 1c, e) and consists mainly of steeply dipping epidote-bearing amphibolites, which are interbedded with layers (up to ~1m in thickness) of leucocratic gneisses (Patzak *et al.* 1994). The stratigraphical range of this sequence is unknown. The contact to the neighbouring subunits is not visible due to the buildings on the site. The geochemical characteristics of the amphibolites indicate basaltic protoliths with a transitional composition between N-MORB and E-MORB or OIT, while the gneisses were associated with Ca-rich greywackes (Patzak *et al.* 1994). *P–T* estimates indicate metamorphic pressures of 0.6–0.85 GPa and temperatures of ~490–610°C (Patzak *et al.* 1994). K–Ar hornblende dating of amphibolites yielded apparent ages of *c.* 77–66 Ma, and white mica of two gneisses provided K–Ar dates of *c.* 59 Ma and *c.* 52 Ma, respectively (Patzak *et al.* 1994).

The Upper subunit (with a thickness of at least 750m) is exposed in six major outcrop areas scattered across the island (Fig. 1c; Melidonis, 1980; Katzir *et al.* 1996; Zeffren *et al.* 2005; Lamont *et al.* 2020a; Mavrogonatos *et al.* 2021). These locations expose lenses and slices (up to several hundred metres in size) of serpentinites, meta-gabbros, meta-plagiogranites, amphibolites, meta-ophicalcites and listvenites that are embedded in or structurally underlain by mostly mafic phyllites (Melidonis, 1980; Katzir *et al.* 1996; Bröcker & Franz, 1998; Zeffren *et al.* 2005; Hinsken *et al.* 2017; Lamont *et al.* 2020a; Mavrogonatos *et al.* 2021). The Upper subunit shows no signs of HP/LT metamorphism and is considered to belong to the Upper Cycladic Unit (e.g. Katzir *et al.* 1996; Bröcker & Franz, 1998; Zeffren *et al.* 2005). The metamorphic history of the various rock types includes upper greenschist to amphibolite-facies ocean floor metamorphism, greenschist-facies overprinting during Oligocene-Miocene orogenic processes, and formation of a metamorphic sole with local partial melting (Katzir *et al.* 1996; Bröcker & Franz, 1998; Zeffren *et al.* 2005; Lamont *et al.* 2020a). According to Lamont *et al.* (2020a), the Upper subunit comprises the Tsiknias ophiolite and the associated metamorphic sole, which includes several thrust sheets consisting mainly of amphibolites (~150 m thick), epidote amphibolites and various metasediments (up to 200 m), respectively, which show an inverted metamorphic gradient from ~0.85 GPa and 850–600°C to greenschist-facies conditions. Previously, Bröcker & Franz (1998) had suggested that the phyllite/meta-gabbro/serpentinite sequence indicates a ductile shear zone that was active during the tectonic stacking onto the Cycladic Blueschist Unit. The Akrotiri subunit has been considered as an exotic block of unknown origin in this mélange or as remnant of a separate tectonic unit belonging to the mostly small, but widely distributed occurrences of Late Cretaceous rocks of the greater Aegean region (Bröcker, 1990; Patzak *et al.* 1994).

Whole-rock compositions of the sole amphibolites indicate affinities to either E-MORB or IAT protoliths (Lamont *et al.* 2020a). U–Pb zircon dating of an amphibolite from the Tsiknias area yielded a protolith age of *c.* 190 Ma (Lamont et al 2020a). Based on Jurassic U–Pb zircon protolith ages for a plagiogranitic sill (*c.* 162 Ma) and a meta-gabbro (*c.* 144 Ma), Lamont et al (2020a) inferred a correlative relationship to the Pelagonian ophiolites of the Greek mainland. Zircons of leucodioritic melt pockets in the sole amphibolites yielded a zircon overgrowth U–Pb age of 74.0 ± 3.5 Ma (Lamont *et al.* 2020a), which overlaps with the K–Ar dates of the Akrotiri amphibolites (Patzak *et al.* 1994).

K–Ar, ^{40}Ar–^{39}Ar and Rb–Sr dates of other rock types (mafic and pelitic phyllites, meta-gabbros) range from 95 to 13 Ma and were interpreted to indicate variable age resetting during juxtaposition-related ductile deformation (Bröcker & Franz, 1998; Zeffren *et al.* 2005). The Upper subunit had been emplaced on top of the Cycladic Blueschist Unit by a low-angle normal fault (e.g. Avigad & Garfunkel, 1989; Katzir *et al.* 1996; Brichau *et al.* 2007). On the basis of a Rb–Sr white mica age of a metapelitic phyllite collected near the tectonic contact and a general downward younging trend towards the Cycladic Blueschist Unit, it was suggested that tectonic stacking of the Upper subunit onto the Cycladic Blueschist Unit occurred in the Miocene (*c.* 21 Ma) (Bröcker & Franz, 1998: Zeffren *et al.* 2005).

2.c. The Vari and greenschist subunits of Syros

On Syros, two tectonic subunits lie structurally above the Cycladic Blueschist Unit (Fig. 1d, f). The uppermost Vari subunit consists mainly of upper greenschist to epidote-amphibolite-facies orthogneisses and a volumetrically subordinate sequence of amphibolites, felsic gneisses and pelitic schists, while the underlying Upper

https://doi.org/10.1017/S0016756824000219 Published online by Cambridge University Press

subunit consists of various greenschist-facies rocks and serpentinites (e.g. Ridley, 1984; Keay, 1998; Keiter *et al.* 2011; Soukis & Stockli, 2013; Aravadinou & Xypolias, 2017). Both subunits were apparently not subjected to HP/LT metamorphism and most likely represent down-faulted tectonic slices (Ridley, 1984; Soukis & Stockli, 2013; Aravadinou & Xypolias, 2017). The interpretation that the Vari subunit represents an allochthonous Pelagonian unit below the Syros HP/LT sequences (Bonneau *et al.* 1980a; Philippon *et al.* 2011) has not found wide acceptance. Most studies conclude that the Vari subunit is separated from the underlying Cycladic Blueschist Unit by a low-angle normal fault (Ridley, 1984), which is not directly exposed, but only roughly marked by the partially mylonitic Upper subunit at the base of the Vari gneiss (Bröcker & Enders, 2001; Keiter *et al.* 2011; Soukis & Stockli, 2013; Aravadinou & Xypolias, 2017). Compared to the Upper subunit on Tinos, which has a wider distribution, greater thickness, greater lithological diversity and includes larger blocks (up to several hundred metres in size), only small remnants of a greenschist subunit are preserved on Syros. Based on zircon fission-track data from HP/LT samples of the footwall on Syros and Tinos, Ring *et al.* (2003) argued that the detachment at its base was active at *c.* 9–12 Ma and responsible for the last ~6–9 km of exhumation of the Cycladic Blueschist Unit on these islands.

Ionprobe U–Pb zircon dating revealed early Triassic (*c.* 244–240 Ma) protolith ages for the Vari gneiss, described as meta-trondjhemite by Keiter *et al.* (2011), and also provided evidence for inherited age components (*c.* 341 Ma) (Keay, 1998; Tomaschek *et al.* 2000b). The inferred intrusion of the Vari gneiss precursor into a quartzo-pelitic sequence (Bonneau *et al.* 1980a, 1980b; Maluski *et al.* 1987) is difficult to verify under the current outcrop conditions, but possible relicts of original country rocks are exposed near Azolimnos (Keiter *et al.* 2011). Geochemical characteristics of the Vari gneiss have not yet been investigated in detail, but the available trace element data indicate an affinity to a volcanic-arc setting (M. Engel, unpub. Ph.D. thesis, Univ. Mainz, 2006; F. Tomaschek, unpub. Ph.D. thesis, Univ. Münster, 2009). Metamorphic *P–T* conditions of the Vari subunit (~1.1 GPa, 550°C; Tomaschek *et al.* 2000a) indicate higher pressures than those reported from the Akrotiri subunit (Patzak *et al.* 1994). White mica geochronology ($^{40}Ar/^{39}Ar$ and Rb–Sr) and a zircon overgrowth (U–Pb) have provided two sets of Late Cretaceous dates (*c.* 99–95 Ma and *c.* 75 Ma) for samples of the Vari gneiss, which have been interpreted as constraints on the timing of upper greenschist- to epidote-amphibolite-facies overprinting (Maluski *et al.* 1987; Tomaschek *et al.* 2000a). Maluski *et al.* (1987) speculated that the 48 Ma date of a low-temperature step of an Ar–Ar release spectrum might be related to the disturbance of the isotopic system during tectonic emplacement of the Vari subunit onto the Cycladic Blueschist Unit. These authors also attributed the Ar–Ar age of ~30 Ma of a footwall sample collected near the tectonic contact to this process. Laurent *et al.* (2021) described apparent $^{40}Ar/^{39}Ar$ ages from 144 to 105 Ma for a phengite population and two single-grain Ar release spectra with dates from 80 to 42 Ma and suggested a relationship to deformation for the youngest dates. Rb–Sr mineral data of two felsic gneiss samples analysed by Glodny & Ring (2022) yielded apparent ages of *c.* 50 Ma and *c.* 32 Ma, respectively, which were related to greenschist-facies deformation and mylonitization. No age data are available for samples of the greenschist subunit on Syros.

The structurally lower part of the metamorphic succession is formed by the Cycladic Blueschist Unit, which is not described in detail here. For more information see Keiter *et al.* (2011), Laurent *et al.* (2016), Kotowski *et al.* (2022) and Uunk *et al.* (2022).

3. Field description and Petrography

From an extensive sample collection, we selected 43 gneisses and amphibolites for bulk-rock geochemical analysis. For comparison, samples from Anafi were included because this island has the largest outcrops of the Asterousia nappe within the Cyclades. For mineral chemical characterization 31 samples were selected. In addition, zircon U–Pb dating was carried out on two felsic gneisses from Syros and one sample from Tinos. Mineral assemblages and GPS coordinates of the sampling locations are listed in online Supplementary Table S1. Field photographs and thin section images are shown in Figures 2–6, S1 and S2.

Tinos: There is only one outcrop of the Akrotiri subunit, located on the edge of the main town (Figs. 1c, e, 2). The NW side of a former quarry is accessible from a sports field, but the walls of the outcrop are steep and covered with rock debris in the lower part. In this area, the amphibolitic rocks are mostly well preserved, while the gneisses are more weathered. Relatively fresh felsic rocks are exposed in the southern and eastern coastal outcrops (Fig. 2b–e). The heterogeneous group of quartz- and feldspar-rich rocks consists mainly of weakly foliated, fine- to medium-grained gneisses (mostly <50 cm thick) that are intercalated with amphibolites. The mineral assemblage consists of variable modal proportions of plagioclase, quartz, epidote or clinozoisite, and Ca-amphibole. White mica, titanite, rutile, apatite, and opaque phases are also present. In several samples, the Ca-amphibole is overgrown by a blue amphibole (Fig. 3a, b). Garnet occurs in a few samples, occasionally in aggregates that may represent former lithic fragments (Fig. 3c). Clinopyroxene is only present in sample 6083. Zircon is rare or very small (mostly <30 μm), with only a few exceptions (Fig. 3d).

The amphibolites are moderately to strongly foliated and partially isoclinally folded, melanocratic rocks that occur in massive layers up to several metres thick. In some cases, millimetre- to centimetre-scale layering occurs due to variations in the modal abundance of amphibole, plagioclase or epidote. The amphibolites are generally granoblastic and to a lesser extent nematoblastic in texture. The mineral assemblage consists mainly of Ca-amphibole and plagioclase with variable amounts of epidote, chlorite and quartz. Titanite or rutile, apatite and opaque phases are present as accessory phases. Garnet and clinopyroxene are not present in the samples selected for this study, but at least garnet can be found sporadically in other rocks. In a few samples (e.g. samples 9033, 9080), some Ca-amphibole grains are overgrown by a blue amphibole (Fig. 3e, f). Plagioclase is often sericitized, and somewhat coarser phengite also appears to be associated with plagioclase breakdown. Chlorite after amphibole and calcium carbonate are of secondary origin. Zircon grains, if present at all, are very small.

Syros: The Vari and greenschist subunits are exposed in SE Syros over an area of about 4 km^2 with a total thickness of <100 m (Figs. 1d, f; Soukis & Stockli, 2013; Aravadinou & Xypolias, 2017). Soukis & Stockli (2013) described a sequence of upper greenschist-schist facies meta-volcanosedimentary rocks as well as meta-acidic rocks and quartzites below the Vari orthogneiss and pointed to the similarity of the meta-volcanosedimentary part with the Akrotiri subunit. According to Aravadinou & Xypolias (2017), the Vari subunit comprises felsic orthogneisses over an amphibolite-gneiss complex up to 30 m thick. This sequence is tectonically underlain by a meta-volcanosedimentary subunit (MVS) consisting of quartz and quartz-feldspar schist, mica schist and metamafic rocks (Fig. 1b). The differences in our interpretation of the field

https://doi.org/10.1017/S0016756824000219 Published online by Cambridge University Press

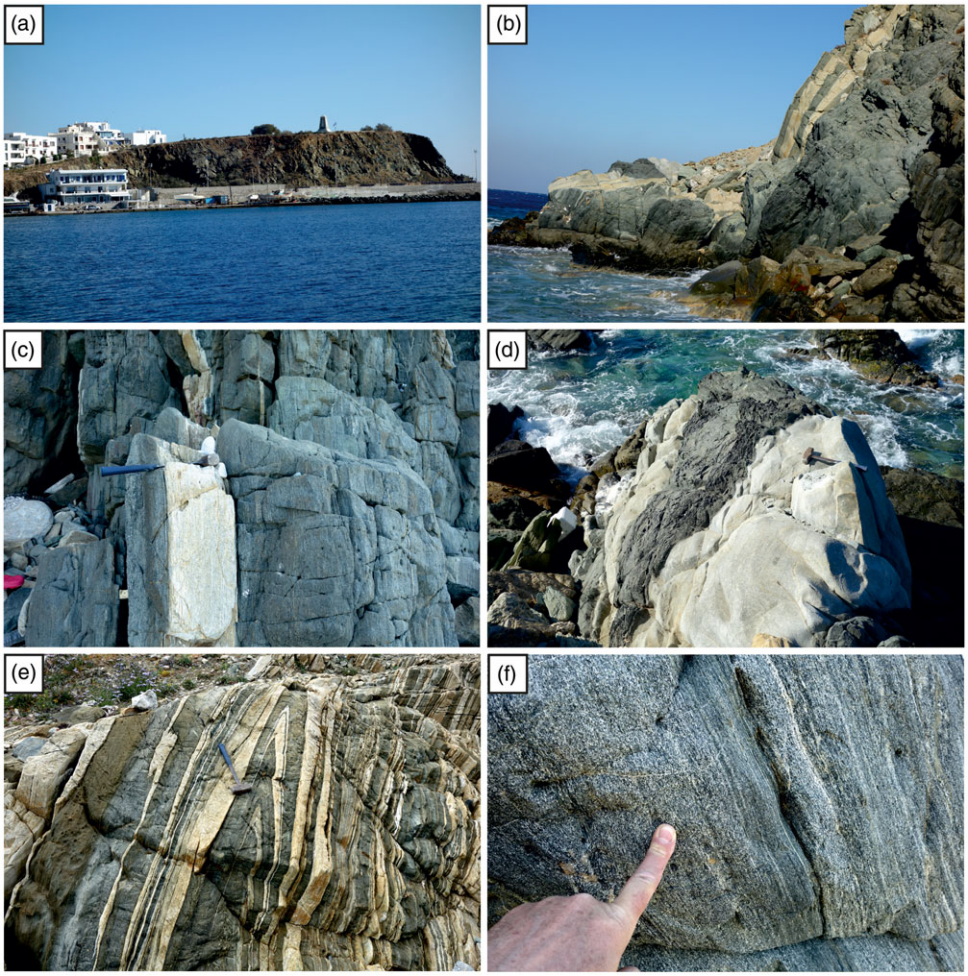

Figure 2. (Colour online) Field images of the Akrotiri subunit, Tinos. (a) General overview of the exposed NW part of the amphibolite-gneiss sequence, which extends no further than 150 m to the left outside the field of view. (b–d) Steeply inclined interlayered amphibolites and felsic gneisses on the southern coastal cliff. (e) Isoclinally folded amphibolite-gneiss sequence on the east coast. (f) Close-up of foliated and finely banded amphibolite. Hammer for scale in (c–e) is 40 cm in length.

relationships compared to these studies concern: (1) the amphibole-rich Cape Phokia gneiss, which was not distinguished from the Vari orthogneiss by Aravadinou & Xypolias (2017) and which we position below the orthogneiss and above the amphibolite-gneiss sequence, unlike Soukis & Stockli (2013), who placed this rock type above the orthogneiss, and (2) the status of the quartz and mica schists, which, in contrast to Aravadinou & Xypolias (2017), we interpret as part of the Vari gneiss complex, as their garnet-bearing mineral assemblages indicate slightly higher *P–T* conditions than the underlying phyllites (Fig. 1b; see also Soukis & Stockli, 2013).

The Vari gneiss sensu strictu (phengite-epidote gneiss) is a medium-grained, strongly foliated rock consisting mainly of quartz, plagioclase, white mica, epidote and minor K-feldspar. Titanite, zircon, apatite and opaque phases occur in variable, but generally small quantities. Secondary alteration is indicated by sericite and chlorite formation. Plagioclase is usually untwinned or has a small number of twin lamellae and often shows deformation-related features reminiscent of exsolution textures of potassic feldspar. Clearly identifiable K-feldspar is characterized by cross-hatched (Tartan) twinning (Fig. 6a), Carlsbad-twins or perthitic exsolution patterns.

The calcic amphibole-rich rocks from Cape Phokia (Fig. 4a–c), which are described here as epidote-hornblende gneisses consist mainly of Ca-amphibole, plagioclase, epidote and quartz (Fig. 6b, c). The abundant chlorite is probably of secondary origin. Titanite, apatite, zircon and opaque phases occur as accessory phases. The relationship to the felsic Vari gneiss is not obvious from field observations. At least locally, the two rock types are separated by a tectonic contact (Fig. 4d). Elsewhere, the different lithologies appear to be in undisturbed contact, with the epidote-hornblende gneiss underlying the Vari gneiss (Fig. 4f).

At Gria Pounta south of Azolimnos (Figs. 1d, f, 5), a sequence of amphibolites, gneisses and mica schists is exposed that may represent the original country rocks of the Vari intrusion (Keiter *et al.* 2011). Parts of this sequence are very similar to outcrops on the east coast of the Akrotiri subunit (Fig. 2; cf. also Soukis & Stockli, 2013). Depending on wind conditions, large parts of the Gria Pounta outcrop are frequently flooded by the sea and many of the rocks are highly altered.

The Gria Pounta amphibolites (Fig. 6d) consist mainly of Ca-amphibole, plagioclase, epidote and quartz. Other phases are chlorite, biotite, titanite, apatite and opaque minerals. The mineral assemblage of the felsic gneisses is dominated by quartz, plagioclase and epidote. Garnet (e.g. sample 9123; Fig. 6e), chlorite, biotite or oxychlorite, white mica, titanite and zircon are typical other constituents. Some samples are richer in quartz, but otherwise there are no significant mineralogical differences, whether collected in direct contact with amphibolites or from layers previously interpreted to belong to the lowest MVS subunit (Aravadinou & Xypolias, 2017). The mineral assemblage of the associated mica schists includes garnet, white mica, chlorite, quartz and plagioclase, opaque phases and zircon (Fig. 6f).

https://doi.org/10.1017/S0016756824000219 Published online by Cambridge University Press

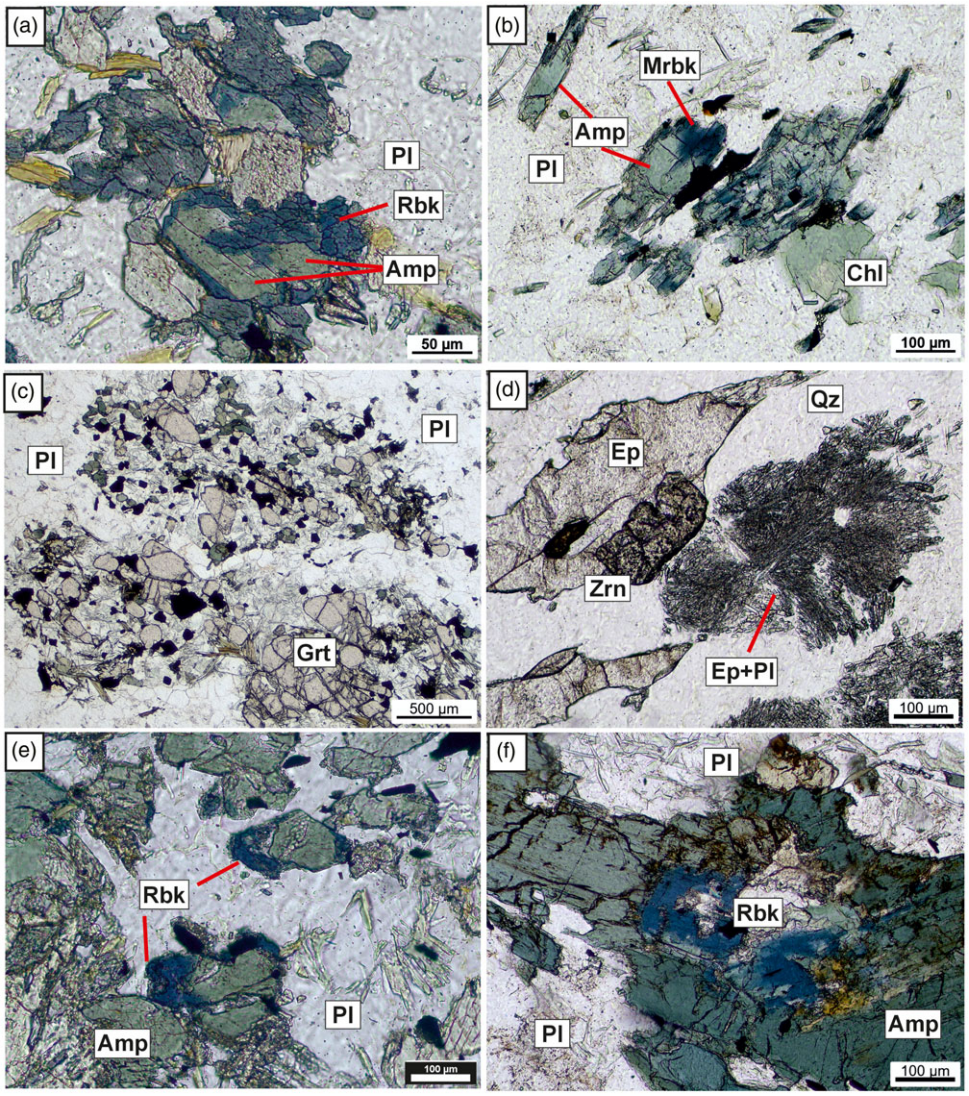

Figure 3. (Colour online) Thin section images of samples from the Akrotiri subunit, Tinos. (a, b) Blue amphibole overgrowths on Ca-amphibole in gneiss samples 8203 and 8208. (c) Garnet-rich domain, possibly replacing lithic fragments, sample 6083. (d) Sample 9083 used for U–Pb geochronology. Plagioclase is filled with numerous fine-grained epidote crystals, which indicates that it was originally an anorthite-rich feldspar. (e, f) Blue amphibole overgrowths on Ca-amphibole in amphibolites 9033 and 9080. Amp = Ca-amphibole; Chl = chlorite; Ep = epidote; Grt = garnet; Mrbk = magnesio-riebeckite; Pl = plagioclase; Qz = quartz; Rbk = Riebeckite; Zrn = zircon.

Greenschists of the Upper subunit, which were not studied in detail here, are weakly foliated in some places and strongly sheared and phyllitic in others. They consist mainly of chlorite, epidote, calcic amphibole and albite. Small amounts of blue amphibole were found in sample 9140 from Santorinious (Fig. S1).

Anafi: The amphibolites are composed mainly of Ca-amphibole and plagioclase (Fig. S2). Quartz, titanite, apatite, tourmaline, and opaque phases occur in small or accessory amounts. Calcic amphibole usually shows no obvious signs of retrogression, whereas plagioclase often shows strong alteration into optically undissolvable stain. Clinopyroxene is present in a few samples and epidote often has a myrmekite-like texture (Fig. S2).

4. Analytical methods

Mineral compositions (Tables S2–S4) were determined with a JEOL 8530F electron microprobe at the Institut für Mineralogie, Universität Münster. Natural and synthetic mineral standards were used for calibration. The operating conditions during the analyses were an electron beam current of 10 nA and an accelerating voltage of 15 kV. The counting times were 10 s for peaks and 5 s for background. A spot size of 5 µm was used for all phases. The raw data were corrected using the PRZ procedure (Armstrong, 1991).

For the preparation of rock powders, fresh sample material was crushed in a steel mortar and an aliquot was ground in an agate mill. The bulk-rock compositions were analysed by ALS, Loughrea, Ireland, using the ICP-AES whole-rock package (lab code ME-ICP06), the lithium borate fusion ICP-MS trace element package (lab code ME-MS81), and the 4-acid digestion ICP-AES package for base metals (lab code ME-4ACD81). For data evaluation and graphical presentation of whole-rock and mineral compositions, Excel and the GeoChemical Data toolkit (GCDkit, version 6.0; Janoušek *et al.* 2006) were used.

For U–Pb geochronology, zircon crystals from three samples (~4–6 kg) were separated by standard routines (jawbreaker, disc mill, Frantz magnetic separator, methylene iodide heavy liquid, and handpicking under stereomicroscope). After the preparation of epoxy resin mounts and polishing to expose grain interiors, cathodoluminescence (CL) images were taken with a JEOL 6510 scanning electron microscope to visualize the internal zircon structures and to guide laser spot placement. The U–Pb measurements on zircon were performed using a sector field ICP-MS (Element 2 and Element XR, Thermo Fisher) coupled to a

https://doi.org/10.1017/S0016756824000219 Published online by Cambridge University Press

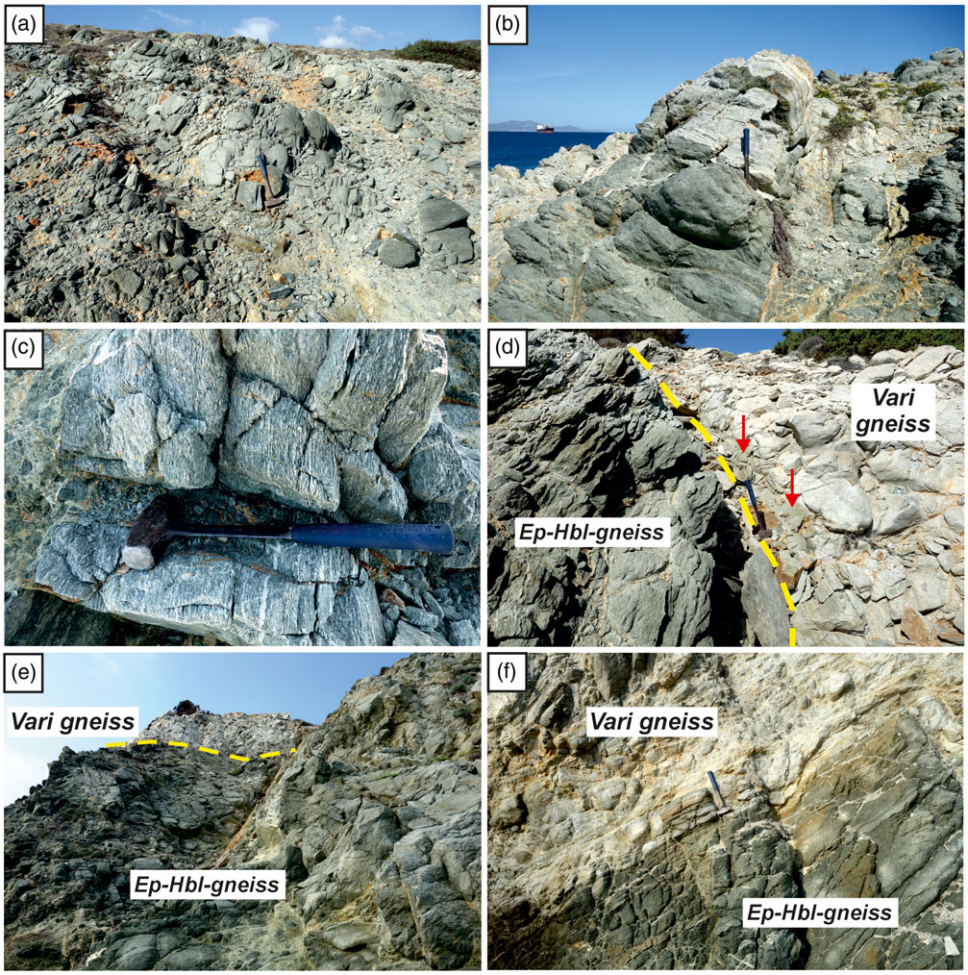

Figure 4. (Colour online) Field images of the epidote-hornblende gneisses from Cape Phokia, Vari subunit, Syros. (a) Overview of the heavily weathered upper part of the outcrop and (b, c) Close-ups of better-preserved gneisses with modal variations of amphibole and plagioclase, resulting in lighter and darker colour variants accentuated by weathering. In general, darker, amphibolite-like gneisses predominate. (d) Tectonic contact between epidote-hornblende gneiss and Vari gneiss sensu strictu. The arrows point to fault gouge. (e, f) Overview and close-up of the lower part of the outcrop seen from a position near the waterline. Hammer for scale in (a–d, f) is 40 cm in length.

193 nm ArF Excimer laser system (Analyte G2, Photon Machines) at the Institut für Mineralogie, Universität Münster, following analytical procedures described in Table S5. Data reduction was performed with the Iolite v.4.8 software (Paton *et al.* 2011). The filtered dataset contains spot analyses with <1% common Pb and <10% discordance. These filters do not exclude any specific age group and have no influence on the overall interpretation of the data. Using the default decay constants and $^{238}U/^{235}U$ ratio, the online version of IsoplotR (Vermeesch, 2018) was used to evaluate and visualize the data in diagrams.

5. Results

5.a. Mineral chemistry

A complete mineral chemical characterization of the samples examined is beyond the scope of this study. The focus here is on the compositions of amphibole and feldspar, which are shown in Figure 7 and Tables S2, S3.

The calcic amphiboles of the Akrotiri amphibolites exhibit a compositional spectrum ranging from pargasite to magnesio-hornblende and tschermakite, but are usually very homogeneous within a sample (Fig. 7a). Tremolite was only recognized in sample 9033. Particularly noteworthy is the occurrence of blue overgrowths with riebeckite composition around green amphiboles in samples 9033 and 9080 (Figs. 3e, f; 7e, f). The plagioclase of the Akrotiri epidote amphibolites is typically albite or oligoclase (Fig. 7h).

The calcic amphibole in the metamafic rocks of Anafi is mainly magnesio-hornblende (Fig. 7b), which occurs together with plagioclase of andesine to labradorite composition (An 41-65; Fig. 7h; Tables S2, S3). The amphiboles of similar rocks from Gria Pounta form a rather uniform group and are mostly classified as magnesio-hornblende or tschermakite and to a lesser extent as pargasite (Fig. 7b). The plagioclase is less rich in anorthite and has mainly an albite to oligoclase composition (Fig. 7h).

The amphibole populations of the gneisses show a somewhat lower homogeneity, but cover a similar compositional range as the amphiboles of the metamafic rocks, and are mostly magnesio-hornblende and tschermakite (Fig. 7c, d). Pargasite is less common. Blue amphibole with a composition of riebeckite to magnesio-riebeckite (Fig. 7e, f) is present in the Akrotiri gneisses 8203 and 8208, as well as in the silicate marble 6070 (see also Patzak *et al.* 1994). In the various Akrotiri gneisses and in the Vari phengite-epidote and epidote-hornblende gneisses, the plagioclase consists mainly of albite, while in the gneisses of Gria Pounta both albite and oligoclase are common (Fig. 7i).

Potassic white mica in the Vari and Gria Pounta gneisses is part of the peak metamorphic assemblage and has Si values in the range of 3.27–3.57 and 3.10–3.65 atoms per formula unit (apfu), respectively (Table S4). White mica is rare in the Akrotiri samples, and the few new analyses for a gneiss and a blue amphibole-bearing amphibolite show Si values between 3.29 and 3.37 apfu, similar to the data reported by Patzak *et al.* (1994) for white mica in gneiss,

https://doi.org/10.1017/S0016756824000219 Published online by Cambridge University Press

Figure 5. (Colour online) Field images of the Gria Pounta outcrop, Vari subunit, Syros. (a) A general view of the south side of the Gria Pounta site. The entire outcrop is confined to this promontory, with the coastal cliffs on either side easily accessible as long as the wind-driven water level allows access. (b-g) Close-ups of the different lithologies. (b) Mica schists in contact with amphibolite-gneiss sequence. (c, d) Interlayered and isoclinally folded amphibolites and gneisses (am-gn). The lower half of the hammer in (d) indicates the position where sample 9123, used for U–Pb zircon geochronology, was collected. (e) Quartz schists (q-sch) between segments of amphibolite-gneiss sequence. (f, g) Close-ups showing continuous transitions between quartz schists and amphibolite-gneiss sequence. Hammer for scale in (c, d, f, g) is 40 cm in length; the backpack in (b, e) is about 45 cm high.

amphibolite and magnesio-riebeckite-bearing silicate marble (~3.3–3.4 apfu).

5.b. Whole-rock geochemistry

The analytical results are presented in Table S6. The loss on ignition (LOI) values range from 0.8 to 2.7 wt%, and for further data evaluation, the major element compositions were recalculated on a volatile-free basis and normalized to 100%. The focus is here on identifying geochemical similarities between the studied occurrences rather than geotectonic classification. As will be explained later, we assume that the studied rocks are igneous in nature and represent either typical volcanic and plutonic rocks or detritus essentially derived from such sources.

The amphibolites are characterized by moderate concentrations of SiO_2 (45.8–55.1 wt.%), and Al_2O_3 (mostly 13.4–18.5 wt.%, with the exception of one sample with 8.8 wt.%) as well as varying contents of Fe_2O_3 (mostly 8.5–17.4 wt.%), MgO (3.5–15.4 wt%), CaO (6.7–12.0 wt.%), K_2O (mostly <0.6wt.% but up to 1.8 wt.%) and Na_2O (2.1–5.1 wt.%). Compared to amphibolites from the Akrotiri and Vari subunits, the samples from Anafi have higher TiO_2 (2.3–3.6 wt.% versus ~1–1.9 wt.%) and Fe_2O_3 concentrations (14.6–17.4 wt.% versus 8.5–13.2 wt.%). Six out of eight samples from Tinos have higher Na_2O contents (4.1–4.5 wt.%) than the amphibolites from Syros and Anafi (2.3–3.3 wt.%).

Judging from major element and trace element compositions, the studied amphibolites originate from basaltic protoliths (Fig. 8a, b; Table S6). Modal transitions to more felsic rock types indicate that some metamafic Akrotiri rocks are derived from tuffaceous or volcaniclastic parent material, but these samples were not geochemically analysed. In diagrams used to distinguish different subalkaline magma series (Hastie *et al.* 2007; Ross & Bedard, 2009), the amphibolites from Anafi show tholeiitic characteristics, while samples from Tinos and Syros show an affinity to calc-alkaline rocks (Fig. 8c, d).

On the basis of discriminant analysis, Vermeesch (2006) evaluated the reliability of ternary diagrams for a test database of samples of known tectonic setting. Some of the ternary diagrams that have been particularly successful in classifying basalts with affinity to mid-ocean ridges (MORB), island arcs (IAB) or ocean islands (OIB) are shown in Fig. 9. The studied amphibolites are assigned to the MORB field in four out of five of these diagrams. However, in the modified Th-Hf/3-Ta diagram, the Akrotiri and two Gria Pounta samples are placed in the IAB field (Fig. 9d). In several

https://doi.org/10.1017/S0016756824000219 Published online by Cambridge University Press

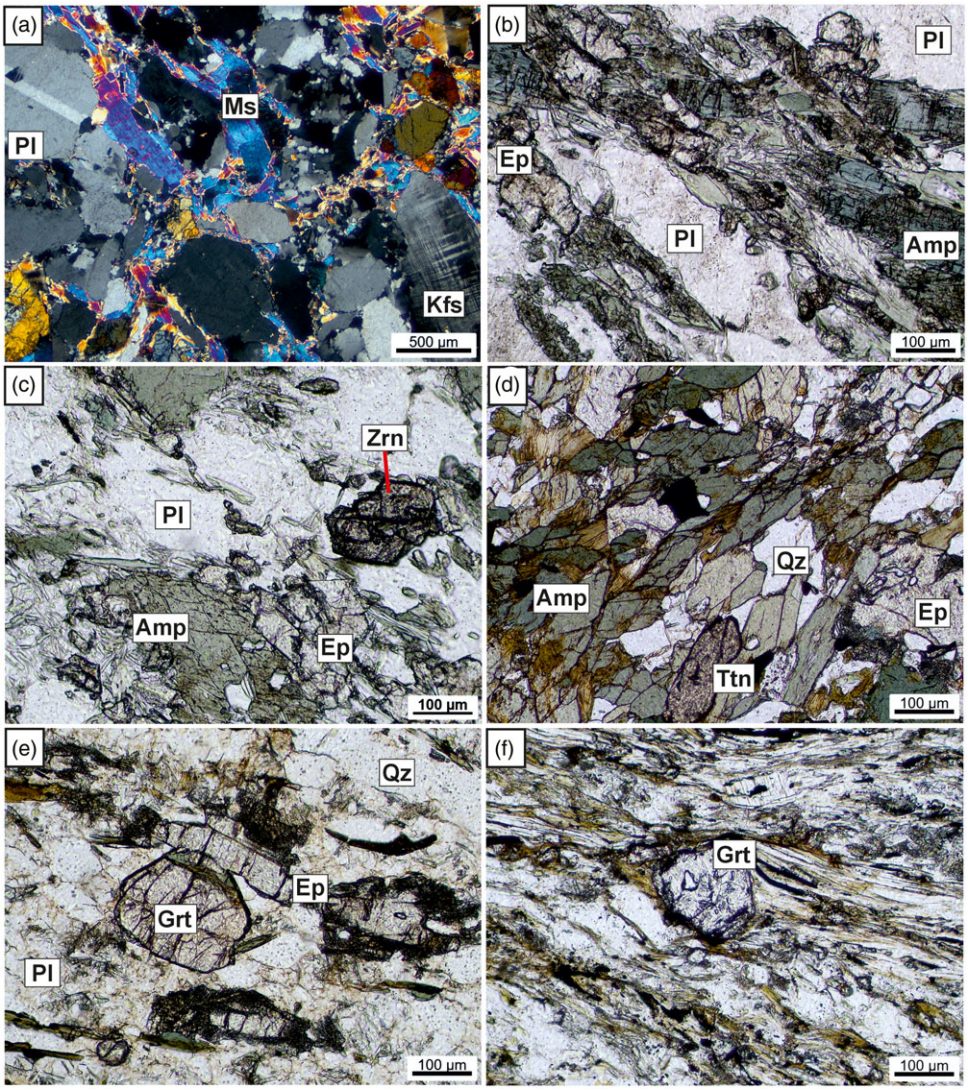

Figure 6. (Colour online) Thin section images of samples from the Vari subunit, Syros. (a) Vari gneiss 9136, south of Gria Pounta; (b, c) Amphibole-rich gneiss from Cape Phokia, (b) sample 9020, (c) sample 9000 used for U–Pb geochronology. (d–f) Samples from Gria Pounta, (d) amphibolite 9013, (e) felsic gneiss 9123 used for U–Pb geochronology, (f) mica schist 9139 with garnet in a white mica-rich groundmass. Amp = Ca-amphibole; Ep = epidote; Grt = garnet; Kfs = K-feldspar; Ms = muscovite; Pl = plagioclase; Qz = quartz; Ttn = titanite; Zrn = zircon.

diagrams, samples representing the Tsiknias metamorphic sole show a different classification than the other amphibolites, with at least two samples showing a clear affiliation to IAB (Fig. 9a, b, e).

The chondrite-normalized rare earth element (REE) diagram for the Akrotiri amphibolites shows a combination of weak light REE (LREE) enrichment relative to heavy REE (HREE) and almost flat distribution patterns. Some samples have a weak negative Eu anomaly (Fig. 10a). The primitive mantle-normalized multi-element diagram displays inconsistent variability on the left end, negative Nb and positive Pb anomalies, and flat patterns from Nd to Lu (Fig. 10b). The Gria Pounta amphibolites show slightly right-inclined, parallel REE distribution patterns with a weak negative Eu anomaly (Fig. 10c). The multi-element spider diagram of the same samples is similar to that of the Akrotiri amphibolites (Fig. 10d). The REE patterns of the Anafi amphibolites display a homogeneous, almost parallel arrangement of lines with ~10–20 times chondritic values and show a weak increase of the LREEs, no or insignificant Eu anomalies and relatively flat, slightly right-inclined HREE distribution (Fig. 10c). The corresponding multi-element distribution patterns are characterized by no or weak negative Nb peaks, positive U, K and Pb anomalies, and flat patterns from Nd to Lu (Fig. 10d). Two of the three Tsiknias amphibolites have REE and multi-element distribution patterns that are similar to the Anafi samples, whereas the third one resembles the Akrotiri patterns (Fig. 10e, f).

Three groups of gneisses can be distinguished. The first group is represented by the mesocratic to melanocratic epidote-hornblende gneiss from Cape Phokia, which has SiO_2 concentrations in the range of 60–69 wt.%, moderate concentrations of Al_2O_3 (13.5–15.3 wt.%), Fe_2O_3 (mostly 5–8 wt.%) and CaO (mostly 4.7–7.8 wt.%), and low concentrations of MgO (2.8–5.1 wt.%), Na_2O (2.5–5.4 wt.%), K_2O (0.7–1.4 wt.%) and TiO_2 (<0.7 wt.%). These samples show an affinity to dioritic rocks or their volcanic equivalents and also include two samples originally described as Vari gneisses for which no petrographic details are available (Fig. 8b). Judging by their geochemistry, it is very likely that these samples belong to the amphibole-rich Cape Phokia-type gneisses.

The second group is formed by the Vari and Gria gneisses from Syros and most gneisses of the Akrotiri subunit. These rocks are characterized by high SiO_2 contents (72.6–78.8 wt.%), moderate Al_2O_3 (12.0–13.6 wt.%), variable CaO (0.8–6.7 wt.%) and Na_2O (2.8–6.9 wt.%) and low Fe_2O_3 (0.6–3.9 wt.%), MgO (0.2–1.1 wt.%) and K_2O (0.1–2.3 wt.%) concentrations. Assuming a

https://doi.org/10.1017/S0016756824000219 Published online by Cambridge University Press

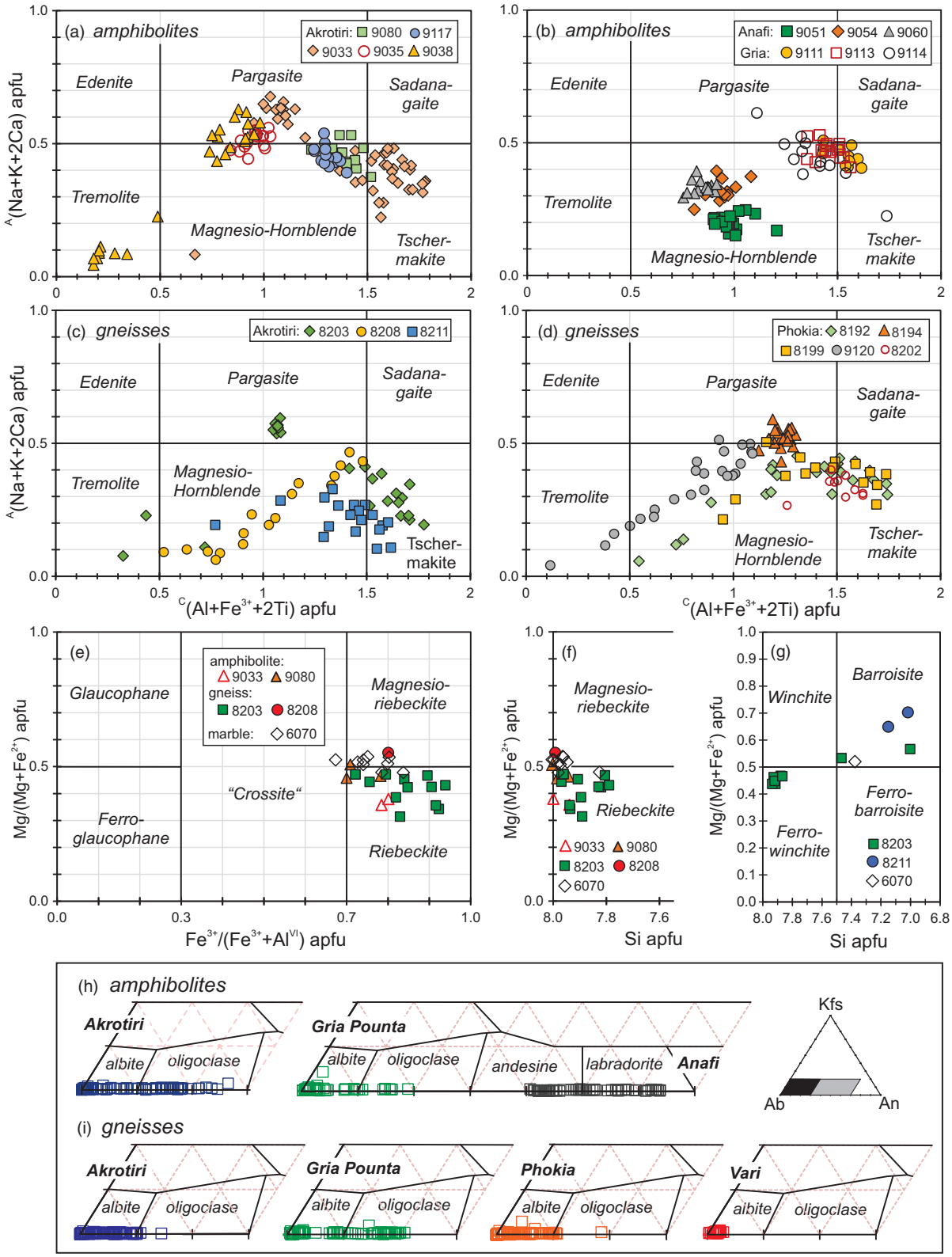

Figure 7. (Colour online) (a–g) Amphibole classification diagrams (atoms per formula unit). (a–d) after Hawthorne *et al.* (2012). (e, f) after Leake *et al.* (1997). (h, i) Close-ups of feldspar compositional ternary diagrams.

predominantly igneous character of the protoliths leads to classify them as granitic rocks sensu lato or their volcanic equivalents (Fig. 8a, b).

The third compositional group comprises three Akrotiri gneisses, which are distinguished primarily by their lower SiO_2 (65.2–66.0 wt.%) and significantly higher Na_2O (8.4–9.9 wt.%)

https://doi.org/10.1017/S0016756824000219 Published online by Cambridge University Press

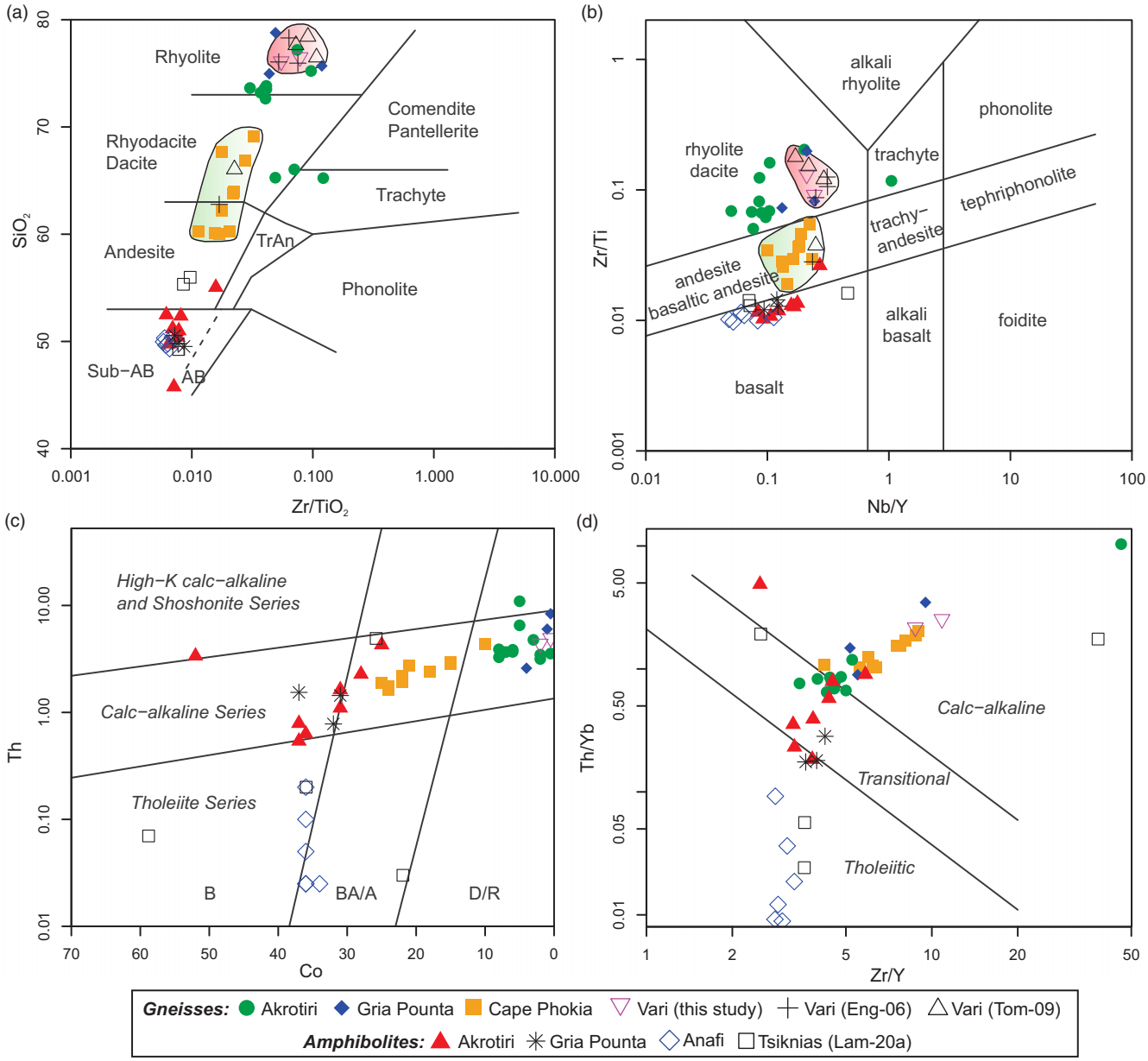

Figure 8. (Colour online) (a, b) Classification of volcanic rocks in the SiO_2 versus Zr/TiO_2 diagram of Winchester & Floyd (1977), and the Zr/Ti versus Nb/Y diagram of the same authors with revised fields of Pearce (1996). Coloured fields show samples that probably represent plutonic rocks or their detritus. (c, d) The Th-Co diagram (Hastie *et al.* 2007) and Th/Yb versus Zr/Y diagram (Ross & Bedard, 2009) for the subdivision of alkalic and sub-alkalic rock series. Eng-06 = M. Engel, unpub. Ph.D. thesis, Univ. Mainz, 2006; Tom-09 = F. Tomaschek, unpub. Ph.D. thesis, Univ. Münster, 2009). Lam-20a = Lamont *et al.* (2020a). TrAn = trachyandesite; B = basalt; BA/A = basaltic andesite/andesite; D/R = dacite/rhyolite.

concentrations. The K_2O concentrations, which are not very high in all gneisses, are particularly low in this group (0.1–0.6 wt.%).

In the CIPW-normative Ab-An-Or diagram for granitic rocks of Barker (1979; not shown), the Vari and Gria gneisses and most Akrotiri samples plot in the trondhjemite field, while the epidote-hornblende gneisses and two of the Akrotiri samples are classified as tonalite. All gneiss samples show calc-alkaline affinities (Fig. 8c, d).

The geochemical granite classification (Frost *et al.* 2001, Frost & Frost, 2008) shows a stronger iron enrichment of the Vari and Gria gneisses and most of the Akrotiri samples compared to the epidote-hornblende gneisses of Cape Phokia (Fig. 11a). Due to the low K_2O concentrations, most of the data points lie in the calcic field (Fig. 11b). The Vari gneisses and many Akrotiri gneisses have a peraluminous composition, but the other half, as well as the samples from Gria Pounta and the dioritic gneisses, are metaluminous (Fig. 11c). The major element discriminant function (DF) diagrams of Verma *et al.* (2012) classify the studied intermediate and silicic rocks as island arc-related granitoids (Fig. 11d–g) and indicate to a lesser extent continental arc affinity (Fig. 11d, h). Assuming that the Akrotiri and Gria Pounta gneisses may be sedimentary rocks that essentially mimic the geochemical characteristics of their igneous source rocks, the DF diagram for the classification of siliciclastic sediments can be used, which indicates affinities to an arc-related tectonic setting (Fig. 11i; Verma & Armstrong-Altrin, 2013).

https://doi.org/10.1017/S0016756824000219 Published online by Cambridge University Press

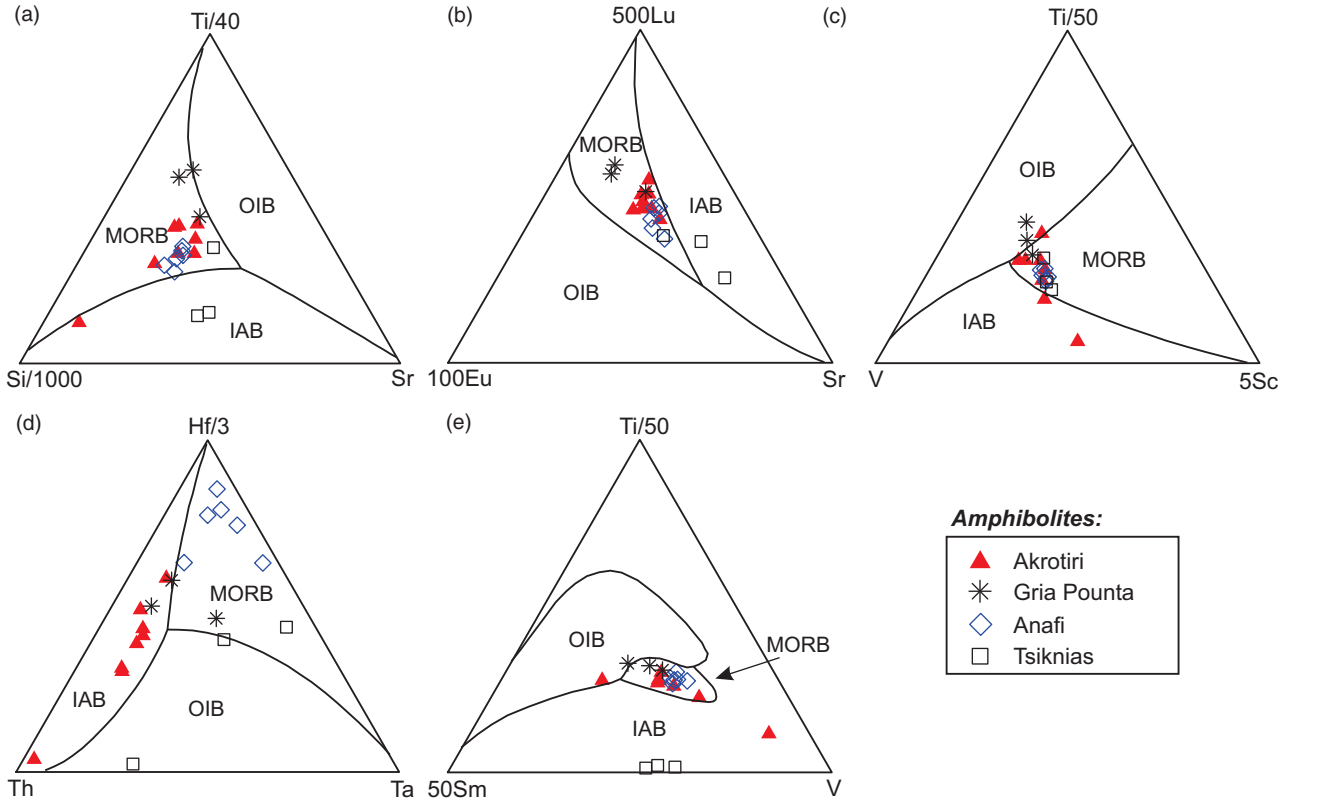

Figure 9. (Colour online) Ternary classification diagrams for mafic volcanic rocks for identification of normal ocean ridge (MORB), island arc (IAB) and ocean island basalts (OIB) (Vermeesch, 2006). Tsiknias data is from Lamont *et al.* (2020a).

In binary trace element diagrams used to distinguish granites from different tectonic settings (Pearce *et al.* 1984) of which only the Yb–Ta and Y–Nb are shown here, the felsic and intermediate gneisses of the Vari subunit plot in the field of volcanic-arc granites (Fig. 11j, k). The same is true for most of the samples from the Akrotiri and Gria Pounta outcrops, which, however, lie close to the field boundary to ocean-ridge granites that cannot be accurately identified with these diagrams (Verma *et al.* 2012; Rollinson & Pease, 2021, p.171).

Chondrite-normalized REE patterns show a strong similarity of the different gneisses from the Akrotiri and Vari subunits, including a moderate LREE enrichment, negligible or negative Eu anomalies and flat HREE distributions. Their primitive mantle-normalized multi-element distribution diagrams display negative Nb, Ta, Sr and Ti peaks (Fig. 12). The epidote-hornblende gneisses have similar REE and multi-element distribution patterns to the other gneisses, but show a pronounced positive Pb peak and negative Nb and Ti anomalies in the multi-element diagrams (Fig. 12f).

5.c. U–Pb geochronology

The U–Pb zircon data obtained by laser ablation inductively coupled plasma mass spectrometry (LA-ICP-MS) are listed in Table S7. Cathodoluminescence (CL) images are shown in Figure 13. Concordia diagrams, kernel density estimates and histograms are presented in Figure 14.

Sample 9083B is a leucocratic gneiss from the Akrotiri subunit (Fig. 3d). The morphologically homogeneous zircon population consists of sub- to euhedral, blocky or short prismatic grains. CL images show many dark or low luminescent crystals with blurred internal structures indicating partially metamict zircons. Better-preserved crystals are characterized by largely homogeneous domains or by growth zoning with some broader bands, as well as a combination of both types (Fig. 13a). Some of the crystals of the 125–63 µm grain-size fraction are mantled by bright luminescent overgrowths that were either too thin to date, or yielded inconsistent apparent ages between *c.* 240–118 Ma. Some of these dates were not considered further due to high analytical uncertainty or elevated common Pb values. The filtered data ($n = 91$) indicate a continuous spectrum of concordant or slightly discordant U–Pb dates from 256 Ma to 114 Ma, with two peaks at *c.* 230 Ma and *c.* 150 Ma (Fig. 14a, b; Table S7). Two individual spots yielded a nominal Permian age (*c.* 256 Ma and *c.* 254 Ma). The oldest apparent age was determined with poor precision for a low uranium, CL-bright overgrowth (273 ± 33 Ma) and is not considered credible. Other CL-bright zircon rims yielded much younger dates (*c.*169–118 Ma) similar to domains with disturbed CL features. In the zircon population as a whole, there is a clear tendency for younger apparent ages to be associated with higher U concentrations (Fig. 14c).

Sample 9123 is a quartz-rich felsic rock from Gria Pounta (Figs. 5d; 6e). The zircon crystals are mostly subhedral to slightly rounded in shape. CL imaging revealed weak oscillatory and sector-zoned patterns, as well as largely homogeneous or banded internal structures, and combinations of these types (Fig. 13b). Distinct overgrowths also occur, but due to their small width and the small grain size, such zones were difficult to analyse without beam overlap on neighbouring zones. The filtered data ($n = 98$) range in age from *c.* 261 Ma to *c.* 127 Ma with a prominent Triassic age cluster around 235 Ma (Fig. 14d, e; Table S7) and eight data

https://doi.org/10.1017/S0016756824000219 Published online by Cambridge University Press

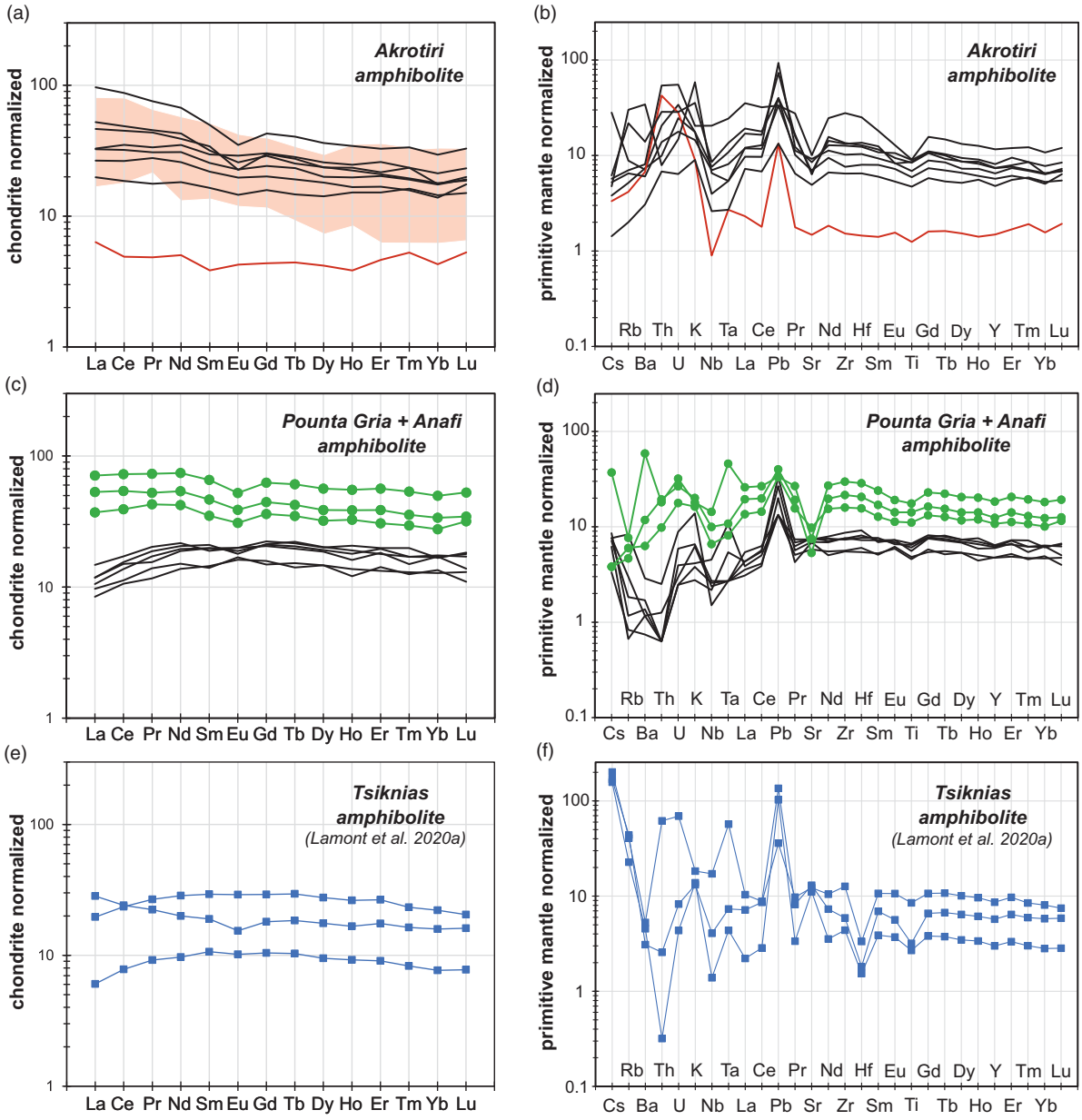

Figure 10. (Colour online) (a–f) Chondrite and primitive mantle (PM) normalized trace element compositions of amphibolites. Normalizing values after McDonough & Sun (1995).

points deviating from the main cluster towards a younger age. The weighted mean $^{206}Pb/^{238}U$ age of the main group is 233.7 ± 2.9 Ma (n = 90; MSWD = 9.4; Fig. 14d). Eight data points with apparent ages of *c.* 193–127 Ma were rejected as outliers in this calculation. Uranium concentrations are mostly in the range from 128–998 ppm, but some grains have U contents up to ~3100 ppm.

Sample 9000 (Fig. 6c) represents the epidote-hornblende gneiss. The homogeneous zircon population consists of sub- to anhedral, blocky or short prismatic grains, which are usually highly fractured. CL imaging shows weakly luminescent grains with oscillatory zoning or broad homogeneous domains (Fig. 13c). Distinct core-rim relationships were not observed. The filtered data (n = 74) show an age range from *c.* 271 Ma to *c.* 217 Ma and a peak around 240 Ma (Fig. 14f, g; Table S7). The weighted mean $^{206}Pb/^{238}U$ age is 238.3 ± 2.1 Ma (n = 74; MSWD = 3.6; Fig. 14f). Uranium concentrations are in the range of 126–958 ppm.

6. Discussion

6.a. Nature and origin of the Akrotiri gneisses

The identification of protoliths of metamorphic rocks is difficult in many cases, because recrystallization and deformation have often completely obscured the pre-metamorphic features, leading to ambivalent interpretations. The geochemical characteristics are also of limited value in determining the origin of such rocks, as in many cases there are overlaps in the composition of possible magmatic and sedimentary precursors. However, under favourable circumstances, characteristics of the zircon population (e.g. crystal shape indicative of transport, age variability associated with different provenance) may allow a clear classification.

Patzak *et al.* (1994) assumed that the Akrotiri gneisses are Ca-rich meta-greywackes, but many of the samples we analysed have relatively low CaO concentrations (<2 wt.%). This could be

https://doi.org/10.1017/S0016756824000219 Published online by Cambridge University Press

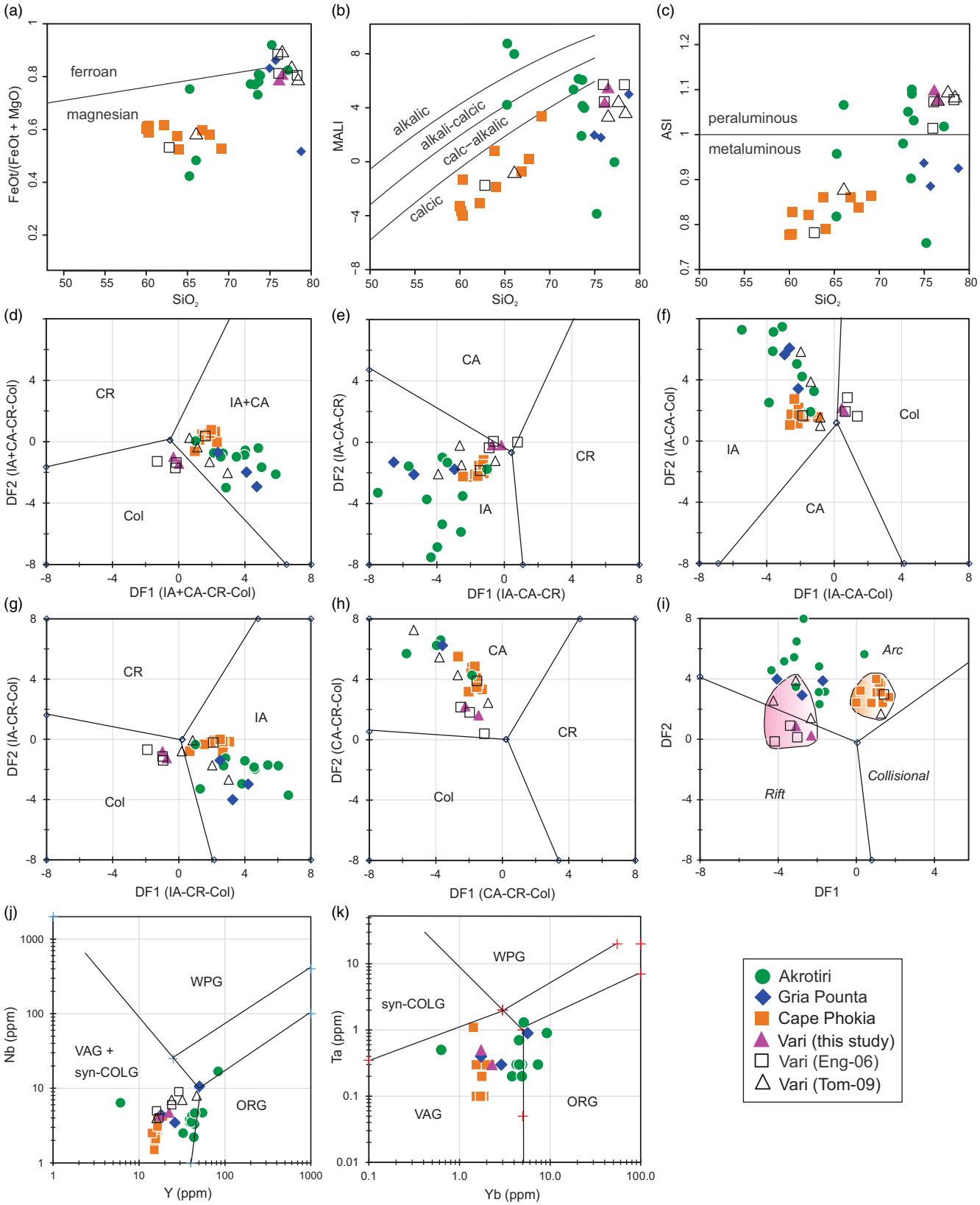

Figure 11. (Colour online) Geochemical classification diagrams of felsic and intermediate gneisses. (a–c) Granite classification using major elements (Frost *et al.* 2001; Frost & Frost, 2008). MALI (modified alkali-lime index) = Na_2O+K_2O-CaO (wt.%); ASI (Aluminium-saturation index) = (Al/(Ca-1.67Ca+Na+K) (molecular). (d–h) Discriminant-function diagrams based on natural log-transformed ratios of major elements for identification of island arc (IA), continental arc (CA), continental rift (CR), and collision (Col) settings (Verma *et al.* 2012). Fe-oxidation was adjusted using the method for plutonic rocks of LeMaitre (1976). (i) Discriminant-function diagram for high-silica clastic sediments (>63 wt.%) from arc, continental rift, and collision settings (Verma & Armstrong-Altrin, 2013). (j, k) Trace element discrimination diagrams for granitic rocks from syn-collision (syn-COLG), volcanic arc (VAG), within plate granites (WPG) and ocean-ridge (ORG) tectonic settings (Pearce *et al.* 1984). Eng-06 = M. Engel, unpub. Ph.D. thesis, Univ. Mainz, 2006; Tom-09 = F. Tomaschek, unpub. Ph.D. thesis, Univ. Münster, 2009).

https://doi.org/10.1017/S0016756824000219 Published online by Cambridge University Press

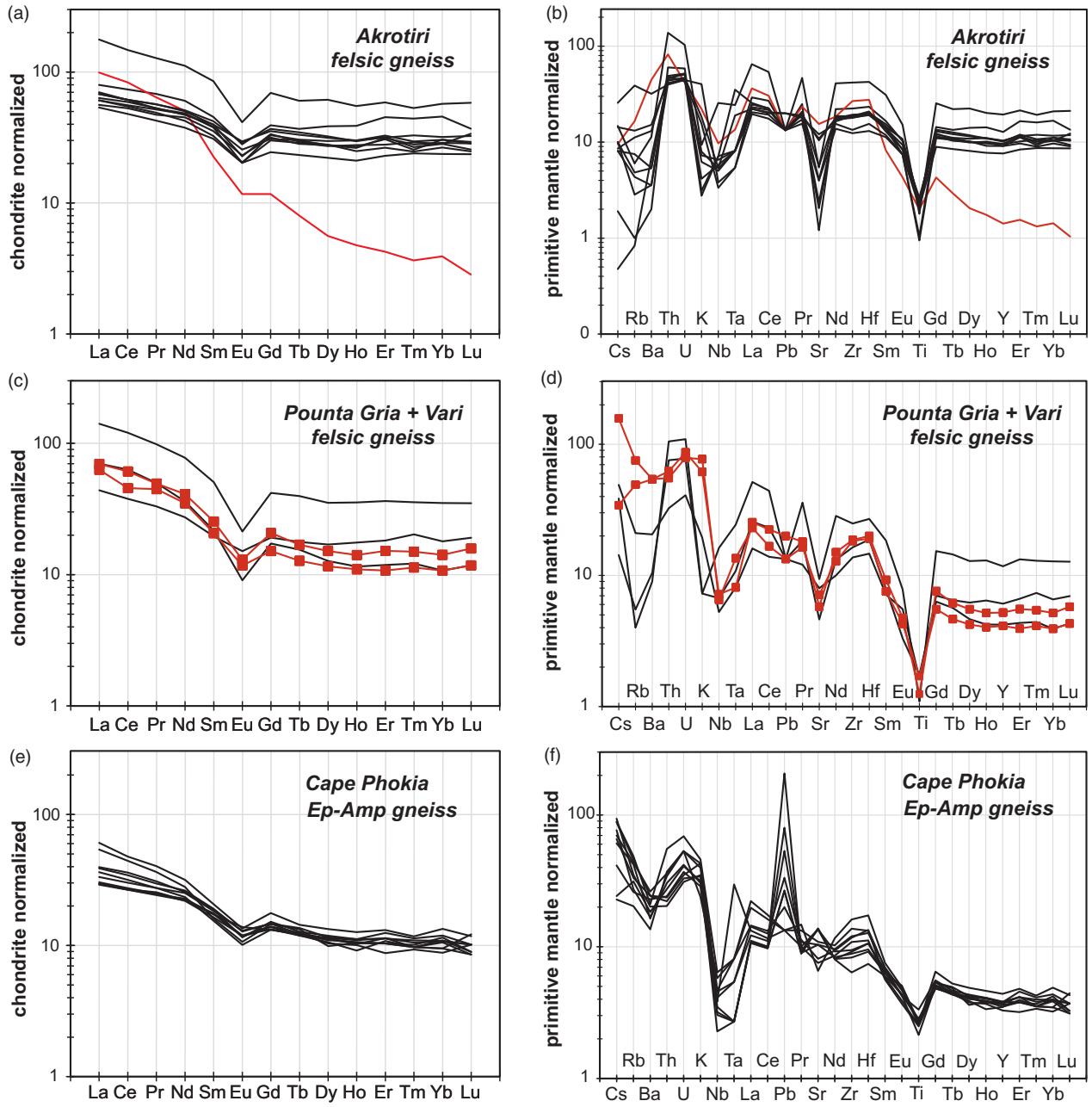

Figure 12. (Colour online) (a–f) Chondrite and primitive mantle (PM) normalized trace element compositions of gneisses. Normalizing values after McDonough & Sun (1995).

due to the different sampling, as the newly analysed gneisses come exclusively from the south and east side of the Akrotiri outcrop, while Patazk *et al.* (1994) worked mainly with samples from the sports field profile. We agree that the Akrotiri gneisses are sedimentary rocks and argue that they were formed mainly from the detritus of sodic plagioclase-rich igneous rocks.

The Akrotiri samples are not well suited for U–Pb geochronology. In most cases, only very small zircons are present, if at all. Only sample 9083 offered sufficiently favourable conditions for U–Pb dating and yielded a complex age spectrum with alignment of the individual data points along the concordia from *c.* 256 to *c.* 114 Ma (Fig. 14a, b). The most likely explanation for this age distribution is either the presence of a detrital zircon population or the existence of a single magmatic population that was affected by variable Pb loss, in both cases complemented by some mixed ages due to beam overlap on different growth zones.

In the first case, the detrital zircons would indicate contributions from Triassic, Jurassic and Cretaceous sources (Fig. 14a, b), probably related to rifting and later arc magmatism, as described for example from the Preveli nappe, which is one of the basal nappes of the Uppermost Unit on Crete (Zulauf *et al.*2023, 2024).

https://doi.org/10.1017/S0016756824000219 Published online by Cambridge University Press

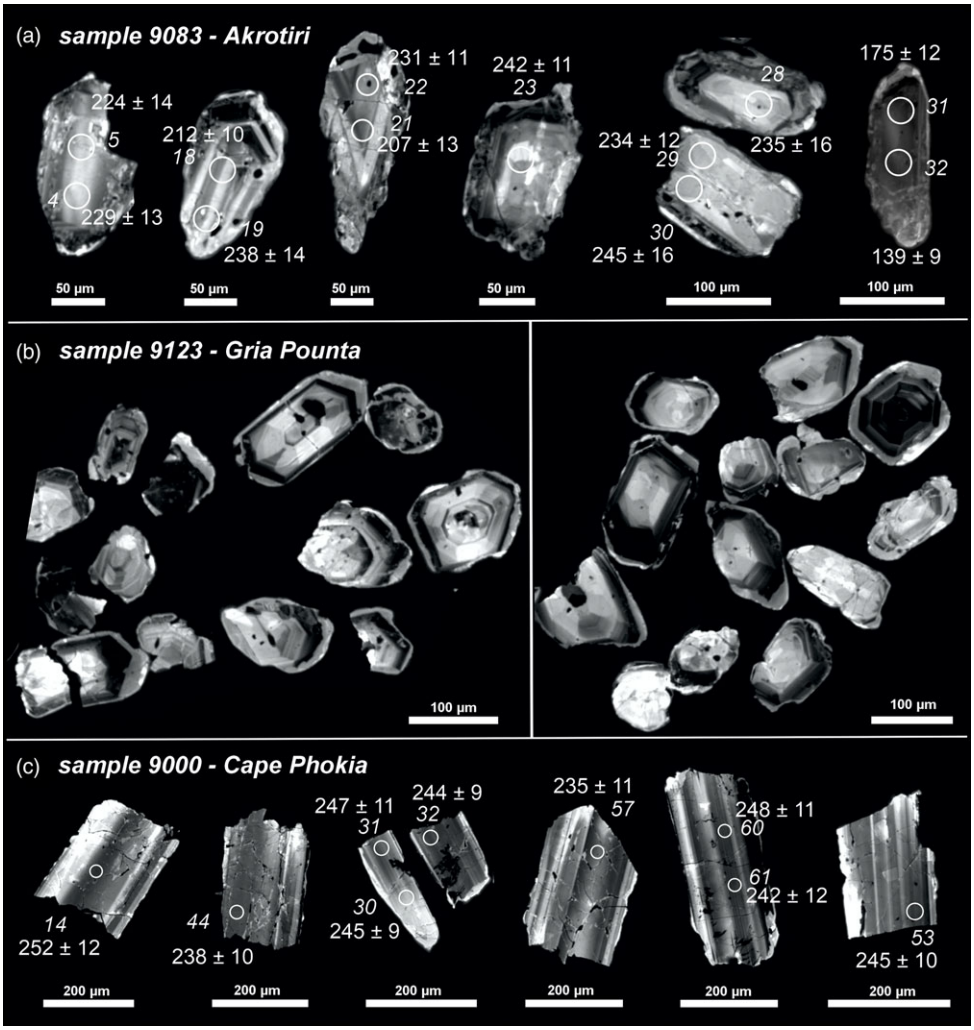

Figure 13. Cathodoluminescence images of representative zircons from U–Pb dated samples from Syros and Tinos with spot identification numbers and $^{206}Pb/^{238}U$ ages (2σ), where available.

However, we consider the second scenario to be more likely, even if this cannot yet be proven beyond doubt. The following points support this view: Most zircons >125 µm have not retained their original zoning and instead show disturbed, CL-dark internal structures, indicating variable degrees of metamictization. In the grain-size fraction <125µm, there is a higher proportion (~50%) of crystals that have largely preserved their original zoning, but the others show convoluted or partially metamict internal structures. Uranium concentrations of the zircons vary widely, ranging from ~70 to ~3900 ppm, and the U content appears to be roughly correlated with apparent age (Fig. 14c). Crystals at the upper end of the age range have lower U contents (<250 ppm) and a latest Permian to Middle Triassic age, whereas most younger ages are observed in combination with higher U contents and poorly preserved internal structures, suggesting that partial metamictization is associated with Pb loss. It cannot be completely ruled out that there was originally only a single magmatic age group that was subject to partial rejuvenation. However, on the basis of the presumed nature of the protolith, we conclude that the zircons in sample 9083 are essentially a detrital population, whose age range is strongly influenced by secondary processes that have displaced many data points along the concordia. It follows that the maximum depositional age cannot be inferred with certainty from the youngest zircons, which may instead indicate the most severe Pb loss. The oldest ages provide a reasonable estimate of the magmatic crystallization age of mainly Triassic source rocks.

It is also important to note that, in contrast to the Vari subunit, no evidence of a metamorphic event at *c.* 95 Ma (Tomaschek *et al.* 2000a) has yet been found in the Akrotiri samples by either U–Pb or K–Ar dating, but the zircon database is very small. Despite extensive sampling, no samples suitable for U–Pb geochronology other than sample 9083 have been found to date.

6.b. Geological significance of blue amphibole in the Akrotiri subunit

All rock types of the Akrotiri subunit on Tinos, including amphibolites, felsic gneisses and impure marbles, occasionally show riebeckite or magnesio-riebeckite overgrowths on pre-existing Ca-amphibole (Fig. 3a, b, e, f; see also Patzak *et al.* 1994). Blue amphibole does not occur in samples from the metamorphic Tsiknias sole (Lamont *et al.* 2020a) or in gneisses and amphibolites of the Vari gneiss subunit. Riebeckite and magnesio-riebeckite provide no evidence for subduction-related metamorphism, but often indicate *P–T* conditions close to the greenschist-blueschist transition (for overviews, see Flores *et al.* 2015 and Manzotti *et al.* 2020, and references therein). Apart from the presence of sodic amphibole, there is no other indication that the Akrotiri rocks were

https://doi.org/10.1017/S0016756824000219 Published online by Cambridge University Press

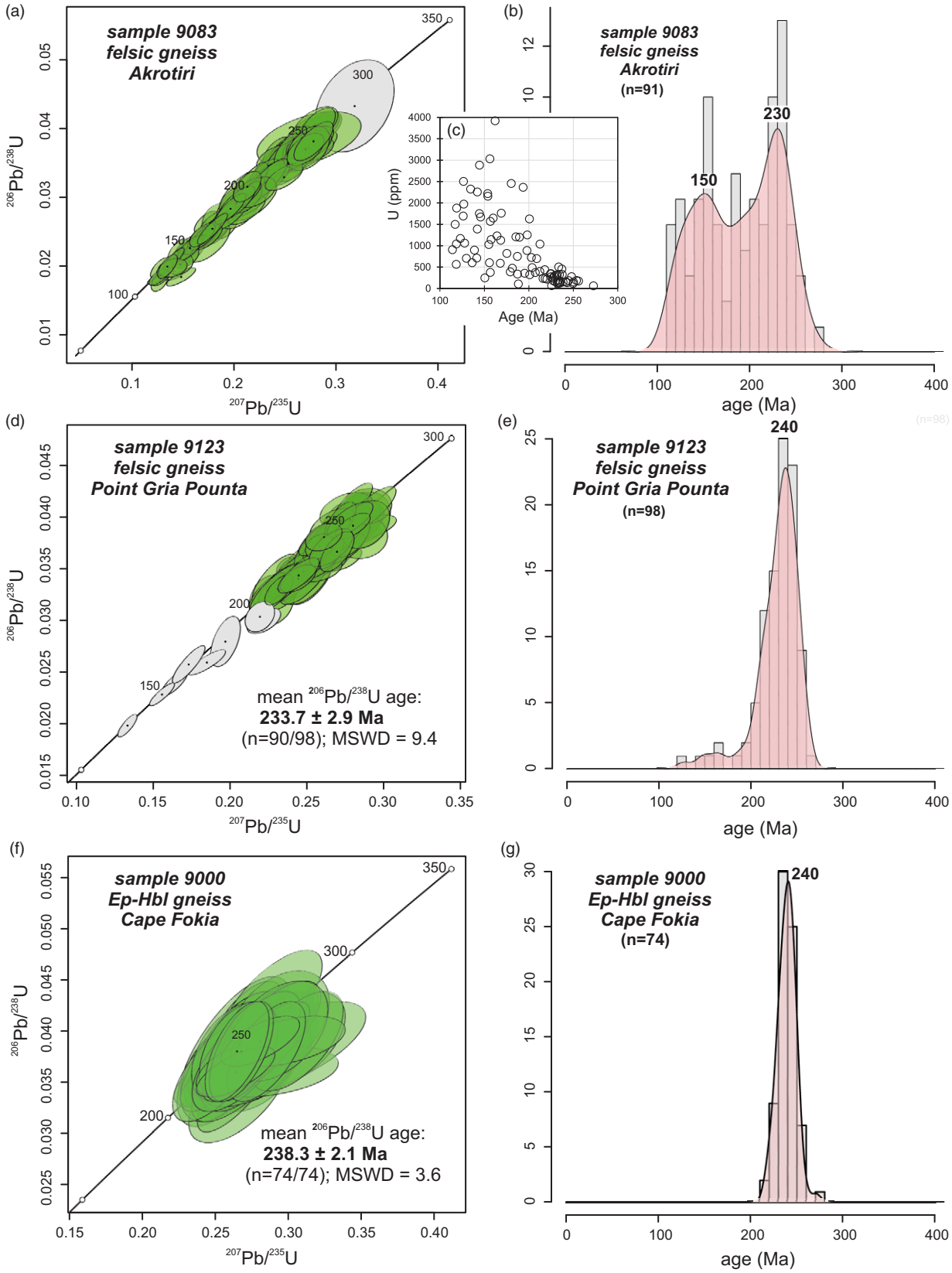

Figure 14. (Colour online) (a, b, d–g) Wetherill concordia diagrams and Kernel density estimates of U–Pb dated samples from Syros and Tinos. (c) Uranium concentration of zircon vs. apparent age (Ma). Data point error ellipses in the concordia diagrams indicate 2σ uncertainties. Weighted mean ages are reported at 95% confidence level. Due to its low precision, the oldest data point in (a) is considered to be of questionable geological relevance. Grey ellipses in (d) indicate data points that were rejected as outliers in the calculation of the weighted mean by IsoplotR.

https://doi.org/10.1017/S0016756824000219 Published online by Cambridge University Press

exposed to pressures higher than those reached during the main phase of the amphibolite-facies overprint (~0.65–0.8 GPa; Patzak *et al.* 1994). The rare clinopyroxene (gneiss sample 6083) is diopside, and the few newly analysed phengites, which are possibly of secondary origin, have Si values (<3.4 apfu).

We also found blue amphibole in a sample of the greenschist subunit on Syros near Santorinious (Fig. S1), suggesting that either fragments of the Cycladic Blueschist Unit may have been tectonically incorporated into the shear zone beneath the Vari gneiss, or that at least parts of the greenschist subunit have a metamorphic history similar to that of the Akrotiri rocks. The timing of this metamorphic episode remains unclear. On Tinos, this event must be younger than the age of the amphibolite-facies stage (*c.* 77–66 Ma), and could possibly be related to the processes recorded by younger K–Ar white mica ages of two Akrotiri gneisses (*c.* 59 Ma and *c.* 52 Ma; Patzak *et al.* 1994).

6.c. Is the Akrotiri unit part of the Tsiknias metamorphic sole?

Metamorphic soles (<500 m thick), consisting mainly of metamorphosed mafic rocks and to a lesser extent of pelagic metasediments, are found below many ophiolite complexes (e.g. Wakabayashi & Dilek, 2000, 2003; Agard *et al.* 2016; van Hinsbergen *et al.* 2015). These metamorphic soles, formed from upper crustal material of the descending plate welded to the mantle section of the upper plate, often exhibit an inverse metamorphic gradient from granulite and high-grade amphibolite-facies conditions in the upper part to lower *P–T* regimes in deeper layers, due to successive underthrusting of younger rocks (e.g. Wakabayashi & Dilek, 2000, 2003; Agard *et al.* 2016; van Hinsbergen *et al.* 2015). Due to the geographical proximity and the similarities in degree of metamorphism and age, it initially seems plausible that the amphibolite-facies Akrotiri rocks could be fragments of the metamorphic sole of the Tsiknias ophiolite. However, there are also differences between the two occurrences: High-grade amphibolites associated with partial melting occur on Tinos only in the Tsiknias area. There is no amphibolite-gneiss sequence in the metamorphic sole, which corresponds lithologically to the Akrotiri rocks. Blue amphibole is present in all Akrotiri lithologies, but is not observed in the Tsiknias area. Geochemically, the Tsiknias amphibolites appear to belong to an independent group that is, however, heterogeneous in itself. There is at least one subgroup which, judging by the REE and multi-element distribution patterns and the ternary discrimination diagrams, is clearly distinct from the Akrotiri samples (Figs. 9, 10). Moreover, given the striking field and petrographic similarities between the two uppermost subunits on Tinos and Syros, which occur in the same tectonic position above the Cycladic Blueschist Unit on both islands, this would inevitably imply that the latter also belongs to the metamorphic sole of the Tsiknias ophiolite. We do not consider this to be a realistic interpretation and rather suspect that the partial correspondence in metamorphic age and degree of metamorphism between the Akrotiri subunit and the Tsiknias metamorphic sole is due to Late Cretaceous processes that occurred simultaneously in different parts of the Aegean subduction-collision complex. Although it cannot be completely ruled out that these are rocks that formed at a greater distance from the overlying ophiolite than the rocks exposed in the Tsiknias area, we consider it unlikely that the Akrotiri rocks represent a fragment of the Tsiknias metamorphic sole, as suggested by Lamont *et al.* (2020a) and instead regard them as a separate tectonic subunit (see also Katzir et al. 1996). Even though there are obviously plausible interpretations of individual aspects, the overall picture is still incomplete, mainly because detailed and reliable geochronological data on the age of the protolith and the metamorphic history of the Akrotiri and Tsiknias rocks are not available to the extent that would be necessary for a comprehensive understanding.

6.d. Protolith origin and age of the Gria Pounta gneisses

At Gria Pounta, there is an outcrop of amphibolites, felsic gneisses and mica schists (Figs. 1d, f, 4). Due to the proximity of this site to the Vari gneiss, it has been hypothesized that the amphibolite-gneiss association of this locality may reflect the injection of aplitic melts from the presumed Vari intrusion into metamafic rocks that were later isoclinally folded together with their host rocks (e.g. Keiter *et al.* 2011). Ionprobe U–Pb zircon dating of such a presumed interfolded meta-aplite yielded an age of 242 ± 4 Ma (2σ; Tomaschek *et al.* 2000b). The felsic sample we dated from this occurrence yielded a slightly younger age of 234 ± 3 Ma (Fig. 14d, e) for the main data cluster. The significance of some younger data points is unclear. They may cover the natural age range of an otherwise largely homogeneous detrital population, may provide evidence of unknown metamorphic events, or may indicate partial Pb loss. For a better understanding of the geological significance of the Triassic zircon ages of the Gria Pounta gneisses, three possible explanations must be considered: (1) These ages date the crystallization of zircons from aplitic melts that intruded into the precursor of the Gria Pounta amphibolites and were isoclinally folded together with their host rock, thus establishing a Triassic (*c.* 240–234 Ma) or older protolith age for the metamafic rocks and associated pelitic metasediments. (2) The felsic gneisses represent feldspathic metasandstones derived from proximate and largely homogeneous igneous source rocks. (3) The dated samples are meta-tuffaceous or meta-volcaniclastic rocks. The zircons document the age of their protoliths.

An intrusive relationship between the Vari gneiss precursor and possibly neighbouring country rocks (Bonneau 1980a, 1980b; Maluski *et al.* 1987) is not evident from the field observations, which are severely hampered by the discontinuous outcrop conditions. There is no obvious contact metamorphic zone, nor are there any aplitic or pegmatitic vein systems that cut through presumed country rocks at Gria Pounta. Although the isoclinal folding of the amphibolite-gneiss sequence is beyond question, there are no conclusive observations to imply that these gneisses were formed from aplitic melts. In our view, this explanation is highly speculative and unlikely. An intrusive relationship cannot be inferred solely from the age correspondence with the precursor of the Vari gneiss. Triassic U–Pb zircon ages have been described from many parts of the Aegean region. For example, felsic layers from bimodal meta-tuffaceous HP/LT rocks collected near Gria Pounta in the underlying unit yielded a Late Triassic age (243 ± 2 Ma), which is indistinguishable from the age of the Gria Pounta sample assumed to represent a meta-aplite (Tomaschek *et al.* 2000b). Similarly, felsic rocks from a layered sequence of felsic gneisses and glaucophanites from the Kampos mélange in the north of Syros yielded U–Pb zircon ages of 245.3 ± 4.9 Ma and 240.1 ± 4.1 Ma (Bröcker & Keasling, 2006). Keay (1998) reported U–Pb zircon data for two very siliceous rocks (described as quartzite) from Naxos that contain zircon populations with a single age peak at about 240–220 Ma and concluded that the limited age range of these zircons, which show little evidence of transport, indicates the incorporation of volcanic detritus from a nearby source. Elsewhere in the larger region, for

https://doi.org/10.1017/S0016756824000219 Published online by Cambridge University Press

example in the nappe stack of the Uppermost Unit on Crete, Triassic U–Pb ages have also been reported for zircon of felsic meta-volcanic rocks from bimodal sequences of the Preveli nappe (Zulauf *et al.* 2023, 2024). Furthermore, as already noted by Soukis & Stockli (2013), there are striking field and lithological similarities between the Gria Pounta and Akrotiri outcrops (Figs. 2, 4), suggesting a similar origin, but there is no evidence of a potential genetic relationship between the Akrotiri gneisses and aplitic dykes of a granitic intrusion.

The second and third possibilities offer more plausible explanations for the origin of the bimodal Gria Pounta sequence, but a clear assignment to one of these alternatives is not readily possible. Some zircons of the newly dated Gria Pounta sample 9123 show rounded grain shapes, but the dominance of poorly abraded zircons with narrowly defined ages and the high modal feldspar cannot be reconciled with long-distance transport, suggesting that this type of material was formed from detritus of felsic igneous rocks from a nearby source with limited age variability, with little mixing with other sedimentary material. In other words, the Gria Pounta gneisses could be sedimentary rocks that largely mimic the mineralogical and geochemical properties of the original plutonic rocks. The boundaries between the felsic and mafic layers are sharp, which at first glance seems to argue against possible mixing processes, unless the continuous sedimentation is repeatedly interrupted by punctual inputs of mafic volcanic material (or vice versa). It is also worth noting that the very similar Akrotiri amphibolite-gneiss sequence exhibits both types, i.e., modal transitions and sharp boundaries between felsic and mafic rock types (Fig. 2b–e, f).

If the reason for the zircon data points deviating from the main cluster (Fig. 14d) is due to secondary processes, as suspected, then the main Triassic age cluster of the felsic gneiss 9123 would correspond to the maximum depositional age, but relatively small contributions from younger source rocks cannot be excluded. In both cases, this would indicate that the maximum depositional age of the Gria Pounta rock suite is significantly younger (<240 Ma) than the Carboniferous age (*c.* 321–311 Ma) tentatively inferred from the youngest detrital zircon component in the associated mica schists, based on measuring only a few grains (F. Tomaschek, unpub. Ph.D. thesis, Univ. Münster, 2009).

The third possibility, which cannot be distinguished from the previous one on the basis of the available information, is that the bimodal sequence was formed by volcanic activity, with alternating deposition of felsic and mafic meta-tuffaceous or meta-volcaniclastic material. However, this alternative would also require some reworking of at least the felsic material. In summary, we consider it unlikely that the gneisses of Gria Pounta originate from injections of aplitic dykes or sills into a mafic rock sequence, followed by isoclinal folding. Other modes of formation are more likely.

6.e. Does the amphibole-rich gneiss of the Vari subunit indicate a separate magma pulse?

Cape Phokia (Fig. 1d, f, 4) hosts a small occurrence of amphibole-rich rocks with an unclear relationship to the neighbouring and more voluminous Vari gneiss. These rocks were previously described as a granodioritic variant of the Vari gneiss protolith (Keiter *et al.* 2011) or as amphibolite (Soukis & Stockli, 2013). The Cape Phokia gneisses are less SiO_2-rich than the Vari gneiss, but have significantly higher SiO_2 concentrations than amphibolites derived from basaltic precursors. The whole-rock composition and the mineral assemblage is consistent with a dioritic protolith and we consider the term 'epidote-hornblende gneiss' to be appropriate. Zircon U–Pb dating of sample 9000 representing this rock type yielded an age of *c.* 238 Ma (Fig. 14f, g). The crystal morphology, the internal CL structures and the individual ages indicate that the zircons originate from a single and homogeneous source and essentially date the time of magmatic crystallization. The apparent protolith age of this rock type is about the same or slightly younger than the ionprobe U–Pb zircon ages reported for the Vari gneiss protolith (*c.* 244–240 Ma), which is usually interpreted to be derived from a granitic or trondhjemitic precursor (e.g. Keay, 1998; Tomaschek *et al.* 2000b; Keiter *et al.* 2011). The epidote-hornblende gneiss could represent a different magma pulse of a more complex granitoid intrusion that also includes the Vari gneiss protolith, or a tectonic sliver of an igneous rock that is unrelated to the precursor of the Vari gneiss. Another alternative results from the petrographic similarity with some rocks of the Akrotiri sequence, which are probably mixtures of mafic and felsic material. Therefore, it is also possible that the epidote-hornblende gneiss is not a true intrusive rock crystallized directly from a melt, but a mixture of materials of different origin and composition, containing only zircons from a single source or from several equally old sources.

6.f. The relationship between the Akrotiri and Vari subunits and their status in the regional context

A correlative relationship between the uppermost subunits on Tinos and Syros is very likely due to similar field, petrographic, geochemical and metamorphic features. On both islands, Late Cretaceous amphibolite-facies rocks occur on top of the metamorphic succession and are tectonically underlain by partly mylonitic, mainly greenschist-facies phyllites, which in turn are separated from the structurally deeper Cycladic Blueschist Unit by low-angle normal faults.

On Tinos, there is no rock body that corresponds lithologically or in size and shape to the Vari gneiss, but felsic to intermediate gneisses, which are quite similar to those of Gria Pounta and Cape Phokia on Syros, are common (Figs. 2, 4, 5). Although it is not yet possible to clearly prove or disprove this conclusion, in our opinion neither the Akrotiri nor the Vari subunits are associated with the metamorphic sole of the Tsiknias ophiolite. We interpret both subunits as part of the scattered occurrences of Late Cretaceous amphibolite-facies rocks of the greater Aegean region. Opinions differ as to whether all these tectonic slices are correctly interpreted as remnants of the Asterousia Crystalline Complex on Crete, which consists mainly of various slices of medium- to high-grade metamorphic rocks (~0.4–0.6 GPa and 700–730°C) including amphibolites, gneisses, mica schists, marbles, calc-silicate rocks and serpentinized ultramafic rocks, locally intruded by granites (e.g. Bonneau, 1972; Seidel *et al.* 1976, 1981; Langosch *et al.* 2000; Bee'ri-Shlevin *et al.* 2009; Martha *et al.* 2016, 2017; 2019; Zulauf *et al.* 2023, 2024). Geochronological studies indicate an Upper Cretaceous age (*c.* 70 Ma) for both metamorphic and intrusive rocks (e.g. Lippolt & Baranyi 1976; Seidel *et al.* 1976, 1981; Kneuker *et al.* 2015; Martha *et al.* 2019 2017; Zulauf *et al.* 2024). The Asterousia nappe is often regarded to correlate with similar rocks in the Upper Cycladic Unit (e.g. Seidel *et al.* 1976, 1981; Dürr *et al.* 1978a; Patzak *et al.* 1994, Bee'ri-Shlevin *et al.* 2009; Martha *et al.* 2016), but there are some differences between the various occurrences in terms of field appearance and metamorphic grade, the significance of which is not fully understood (e.g., Altherr *et al.* 1994; Patzak *et al.* 1994; Langosch et al. 2000; Martha *et al.* 2016;

https://doi.org/10.1017/S0016756824000219 Published online by Cambridge University Press

Pe-Piper & Photiades 2006; Be'eri-Shlevin *et al.* 2009). Earlier studies assumed a correlation of the Late Cretaceous rocks with the Pelagonian Zone of mainland Greece or to magmatic arcs in NW Turkey (e.g. Be'eri-Shlevin *et al.* 2009; Martha *et al.* 2016). Based on detrital zircon data from Crete, Zulauf *et al.* (2024) have recently argued that the Asterousia nappe originated from a Late Permian/Late Cretaceous magmatic belt north of the Sava-Vardar-Izmir-Ankara suture in the Bulgarian-Greek Strandja-Rhodope area, and suggested that the similar rocks in the Cyclades ultimately trace the migration path from the source area to Crete. This is a reasonable interpretation, but due to the limited database (e.g. no or almost no detrital zircon data from Tinos, Syros, Anafi) it remains uncertain at present whether all these occurrences actually belong to a single tectonic unit with regional differences in the tectonometamorphic evolution, or to several with distinct *P–T* histories. In any case, there are striking similarities in the geological records of different tectonic subunits from the upper parts of the central and southern Aegean nappe stacks (e.g. Zulauf *et al.* 2023, 2024). So far there is no convincing evidence for this hypothesis, but future studies should also examine the possibility that the Late Cretaceous amphibolite-facies rocks of the Aegean region may be remnants of a more regional metamorphic sole.

7. Summary and conclusions

Among the results of this study, the following points are particularly noteworthy:

(1) The protoliths of the Akrotiri and Gria Pounta gneisses probably represent variably reworked felsic igneous rocks from a nearby source, derived either from volcaniclastic/pyroclastic material or from detritus of plutonic rocks.
(2) The age range of zircons from an Akrotiri gneiss (*c.* 256–114 Ma) is probably strongly influenced by variable Pb loss. In this particular case, it is not the youngest zircons that determine the maximum depositional age, as they have probably been reset by secondary processes. Crystals at the upper end of the age spectrum that are least affected by the presumed Pb loss largely indicate an Early to Middle Triassic age for the source rock or at least for a substantial part of the parent material.
(3) Sodium amphibole, apparently formed during later overprinting, occurs in small amounts in many mafic and felsic rocks of the Akrotiri subunit and is not largely restricted to the volumetrically subordinate silicate marbles, as described in previous work.
(4) The Triassic U–Pb zircon age (*c.* 240 Ma) of the Gria Pounta gneisses mainly determines the magmatic crystallization age of the source rocks, which are derived from similar protoliths as the Akrotiri gneisses. The significance of the data points with apparent ages of *c.* 193–127 Ma is still unclear and could either be due to a minor admixture of younger rock material or to unspecified secondary processes.
(5) Amphibole-rich gneissic rocks, mainly exposed at Cape Phokia and formerly referred to as meta-granodiorite or amphibolite, have a predominantly dioritic bulk-rock composition. The Triassic U–Pb zircon age (*c.* 238 Ma) of such an epidote-hornblende gneiss is close to the protolith age of the Vari gneiss, consistent with interpretations suggesting a common origin from a composite intrusion. However, its classification as a true plutonic rock is called into question by petrographic similarities with rocks of the Akrotiri subunit, which are interpreted as mixtures of mafic and felsic igneous material.
(6) Although uncertainties remain, a correlative relationship of the Akrotiri subunit with the metamorphic sole of the Tsiknias ophiolite is considered less likely. From all the observations and data, we conclude that it is reasonable to correlate the Akrotiri with the Vari subunit and to assign both to the heterogeneous group of Late Cretaceous amphibolite-facies rocks of the greater Aegean region, which, according to current knowledge, are not associated with metamorphic soles of Pelagonian ophiolites.

Supplementary material. To view supplementary material for this article, please visit https://doi.org/10.1017/S0016756824000219

Availability of data and material. All data are provided in the Supplementary Information of the online version.

Acknowledgements. This research received no specific grant from any funding agency, commercial or not-for-profit sectors. Open Access funding enabled and organized by Projekt DEAL. We thank Maik Trogisch for the preparation of the thin sections and Beate Schmitte for her help with the electron microprobe and the LA-ICP-MS. We would also like to thank Arno Rohrbach and Christian Vollmer for their support with the CL imaging of the zircons. Constructive reviews by Thomas Lamont, Gernold Zulauf and an anonymous referee are gratefully acknowledged.

Financial support. Open Access funding enabled and organized by Projekt DEAL.

Competing interests. The authors declare none.

Code availability. Not applicable.

References

Agard P, Yamato P, Soret M, Prigent C, Guillot S, Plunder A, Dubacq B, Chauvet A, Monie P (2016) Plate interface rheological switches during subduction infancy: control on slab penetration and metamorphic sole formation. *Earth and Planetary Science Letters* **451**, 208–220.

Altherr R, Kreuzer H, Lenz H, Wendt I, Harre W and Dürr S (1994) Further evidence for Late-Cretaceous low pressure/high-temperature terrane in the Cyclades, Greece. *Chemie der Erde* **54**, 319–328.

Altherr R, Schliestedt M, Okrusch M, Seidel E, Kreuzer H, Harre W, Lenz H, Wendt I and Wagner GA (1979) Geochronology of high-pressure rocks on Sifnos (Cyclades, Greece). *Contributions to Mineralogy and Petrology* **70**, 245–255.

Aravadinou E and Xypolias P (2017) Evolution of a passive crustal-scale detachment (Syros, Aegean region): insights from structural and petrofabric analyses in the hanging-wall. *Journal of Structural Geology* **103**, 57–74.

Armstrong JT (1991) Quantitative elemental analysis of individual microparticles with electron beam instruments. In *Electron Probe Quantitation* (eds KFJ Heinrich and DE Newbury), pp. 261–315. Boston, Massachusetts: Springer.

Avigad D and Garfunkel Z (1989) Low angle shear zones underneath and above a blueschist belt - Tinos Island, Cyclades, Greece. *Terra Nova* **1**,182–87.

Barker F (1979) Trondhjemite: definition, environment and hypotheses of origin. In *Trondhjemites, Dacites and Related Rocks* (ed F Barker), pp. 1–12. Amsterdam: Elsevier.

Be'eri-Shlevin Y, Avigad D and Matthews A (2009) Granitoid intrusion and high temperature metamorphism in the Asteroussia Unit, Anafi Island (Greece): petrology and geochronology. *Israel Journal of Earth Sciences* **58**, 13–27.

Brichau S, Ring U, Carter A, Monié P, Bolhar R, Stockli D and Brunel M (2007) Extensional faulting on Tinos Island, Aegean Sea, Greece: how many detachments? *Tectonics* **26**, TC4009.

Bonneau M (1972) La nappe métamorphique de l'Asteroussia, lambeau d'affinités pélagoniennes charrié jusque sur la zone de Tripolitza de la Crète moyenne (Grèce). *Comptes Rendus de l'Académie des Sciences, Serié D* **275**, 2303–2306.

Bonneau M, Blake, MC, Gueyssant J, Kienast, JR, Lepvrier C, Maluski H and Papanikolaou D (1980a) Sur la signification des séries métamorphiques (schistes bleus) des Cyclades (Héllenides, Grèce). L'exemple de l'île de Syros. *Comptes Rendus de l'Académie des Sciences, Serié D* **290**, 1463–1466.

Bonneau M, Geyssant J, Kienast JR, Lepvrier C and Maluski H (1980b) Tectonique et métamorphisme haute pression d'age Éocene dans les Héllenides: exemple de l'île de Syros (Cyclades, Grèce). *Comptes Rendus de l'Académie des Sciences, Série D* **291**, 171–174.

Bröcker M (1990) Die Blauschiefer–Grünschiefer-Assoziation der Insel Tinos (Kykladen, Griechenland) und ihre kontaktmetamorphe Überprägung. *Geotektonische Forschungen* **74**, 1–107.

Bröcker M and Enders M (2001) Unusual bulk-rock compositions in eclogite-facies rocks from Syros and Tinos (Cyclades, Greece): implications for U–Pb zircon geochronology. *Chemical Geology* **175**, 581–603.

Bröcker M and Franz L (1998) Rb–Sr isotope studies on Tinos Island (Cyclades, Greece): additional time constraints for metamorphism, extent of infiltration-controlled overprinting and deformational activity. *Geological Magazine* **135**, 369–82.

Bröcker M and Keasling A (2006) Ion probe U–Pb zircon ages from the high-pressure/ low-temperature mélange of Syros, Greece: age diversity and the importance of pre-Eocene subduction. *Journal of Metamorphic Geology* **24**, 615–31.

Bröcker M, Baldwin S and Arkudas R (2013) The geologic significance of $^{40}Ar/^{39}Ar$ and Rb–Sr white mica ages from Syros and Sifnos, Greece: a record of continuous (re)crystallization during exhumation? *Journal of Metamorphic Geology* **31**, 629–646.

Bröcker M, Kreuzer H, Matthews A and Okrusch M (1993) $^{40}Ar/^{39}Ar$ and oxygen isotope studies of polymetamorphism from Tinos Island, Cycladic blueschist belt. *Journal of Metamorphic Geology* **11**, 223–240.

Bröcker M, Bieling D, Hacker B and Gans P (2004) High-Si phengite records the time of greenschist-facies overprinting: implications for models suggesting megadetachments in the Aegean Sea. *Journal of Metamorphic Geology* **22**, 427–442.

Cliff RA, Bond CE, Butler RWH and Dixon JE (2017) Geochronological challenges posed by continuously developing tectonometamorphic systems, insights from Rb–Sr mica ages from the Cycladic Blueschist Belt, Syros (Greece). *Journal of Metamorphic Geology* **35**, 197–211.

Dürr S (1986) Das Attisch-kykladische Kristallin. In *Geologie von Griechenland* (ed V Jacobshagen), pp. 116–148. Berlin: Gebrüder Bornträger.

Dürr S, Altherr R, Keller J, Okrusch M and Seidel E (1978a) The Median Aegean Crystalline Belt: stratigraphy, structure, metamorphism, magmatism. In *Alps, Appeninnes, Hellenides* (eds H Closs, DH Roeder and K Schmidt), pp. 455–477. Stuttgart: Schweizerbart.

Dürr S, Seidel E, Kreuzer H and Harre W (1978b) Témoins d'un métamorphisme d'âge crétacé supérieur dans l'Égéide: datations radiométriques de minéraux provenant de l'île de Nikouriá (Cyclades, Grèce). *Bulletin de la Société Géologique de France* **7**, 209–213.

Flores KE, Skora S, Martin C, Harlow GE, Rodríguez D and Baumgartner PO (2015) Metamorphic history of riebeckite- and aegirine-augite-bearing high-pressure–low-temperature blocks within the Siuna Serpentinite Mélange, northeastern Nicaragua. *International Geology Review* **57**, 943–977.

Frost BR and Frost CD (2008) A geochemical classification for feldspathic igneous rocks. *Journal of Petrology* **49**, 1955–1969.

Frost BR, Arculus RJ, Barnes CG, Collins WJ, Ellis DJ and Frost CD (2001) A geochemical classification of granitic rocks. *Journal of Petrology* **42**, 2033–2048.

Forster MA and Lister GS (2005) Several distinct tectono-metamorphic slices in the Cycladic eclogite–blueschist belt, Greece. *Contributions to Mineralogy and Petrology* **150**, 523–45.

Glodny J and Ring U (2022) The Cycladic Blueschist Unit of the Hellenic subduction orogen: protracted high-pressure metamorphism, decompression and reimbrication of a diachronous nappe stack. *Earth-Science Reviews* **224**. 103883.

Grasemann B, Huet B, Schneider DA, Rice AHN, Lemonnier N and Tschegg C (2018) Miocene postorogenic extension of the Eocene synorogenic imbricated Hellenic subduction channel: new constraints from Milos (Cyclades, Greece). *Geological Society of America Bulletin* **130**, 238–262.

Hawthorne FC, Oberti R, Harlow GE, Maresch WV, Martin RF, Schumacher JC and Welch MD (2012) Nomenclature of the amphibole supergroup. *American Mineralogist* **97**, 2031–2048.

Hinsken T, Bröcker M, Strauss H and Bulle F (2017) Geochemical, isotopic and geochronological characterization of listvenite from the Upper Unit on Tinos, Cyclades, Greece. *Lithos* **282**, 281–297.

Hastie AR, Kerr AC, Pearce JA and Mitchell SF (2007) Classification of altered volcanic island arc rocks using immobile trace elements: development of the Th–Co discrimination diagram. *Journal of Petrology* **48**, 2341–2357.

IGME (2003) Geologic map of Greece. Tinos and Yaros islands, 1:50.000. Institute of Geological and Mining Research, Athens.

Janoušek V, Farrow CM and Erban V (2006) Interpretation of whole-rock geochemical data in igneous geochemistry: introducing Geochemical Data Toolkit (GCDkit). *Journal of Petrology* **47**, 1255–1259.

Jolivet L, Lecomte E, Huet B, Denèle Y, Lacombe O, Labrousse L, Le Pourhiet L and Mehl C (2010) The North Cycladic Detachment System. *Earth and Planetary Science Letters* **289**, 87–104.

Jolivet L and Brun JP (2010) Cenozoic geodynamic evolution of the Aegean. *International Journal of Earth Sciences* **99**, 109–138.

Katzir Y, Matthews A, Garfunkel Z and Schliestedt M (1996) The tectono-metamorphic evolution of a dismembered ophiolite (Tinos, Cyclades, Greece). *Geological Magazine* **133**, 237–254.

Keay S (1998) The Geological Evolution of the Cyclades, Greece: Constraints from SHRIMP U–Pb Geochronology. PhD thesis, Australian National University, Canberra. Published thesis. doi: 10.25911/5d66671ad2b2f

Keiter M, Ballhaus C and Tomaschek F (2011) A new geological map of the Island of Syros (Aegean Sea, Greece): implications for lithostratigraphy and structural history of the Cycladic Blueschist Unit. *Geological Society of America Special Paper* **481**, 1–43.

Keiter M, Piepjohn K, Ballhaus C, Lagos M and Bode M (2004) Structural development of high-pressure metamorphic rocks on Syros island (Cyclades, Greece). *Journal of Structural Geology* **26**, 1433–1445.

Kneuker T, Dörr W, Petschick R and Zulauf G (2015) Upper crustal emplacement and deformation of granitoids inside the Uppermost Unit of the Cretan nappe stack: constraints from U–Pb zircon dating, microfabrics and paleostress analyses. *International Journal of Earth Sciences* **104**, 351–367.

Kotowski AJ, Cisneros M, Behr WM, Stockli DF, Soukis K, Barnes JD and Ortega-Arroyo D (2022) Subduction, underplating, and return flow recorded in the Cycladic Blueschist Unit exposed on Syros, Greece. *Tectonics* **41**, e2020TC006528.

Kuhlemann J, Frisch W, Dunkl I, Kázmér M and Schmiedl G (2004) Miocene siliciclastic deposits of Naxos Island: geodynamic and environmental implications for the evolution of the Southern Aegean Sea (Greece). *Geological Society of America Special Papers* **378**, 51–65.

Lagos M, Scherer EE, Tomaschek F, Münker C, Keiter M, Berndt J and Ballhaus C (2007) High precision Lu–Hf geochronology of Eocene eclogite-facies rocks from Syros, Cyclades, Greece. *Chemical Geology* **243**, 16–35.

Lamont TN, Roberts NMW, Searle MP, Gopon P, Waters DJ and Millar I (2020a) The Age, Origin, and Emplacement of the Tsiknias Ophiolite, Tinos, Greece. *Tectonics* **39**, e2019TC005677.

Lamont TN, Searle MP, Gopon P, Roberts NMW, Wade J, Palin RM and Waters DJ (2020b) The Cycladic Blueschist Unit on Tinos, Greece: cold NE subduction and SW directed extrusion of the Cycladic continental margin under the Tsiknias Ophiolite. *Tectonics* **39**, e2019TC005890.

Langosch A, Seidel E, Stosch HG and Okrusch M (2000) Intrusive rocks in the ophiolitic mélange of Crete – witnesses to Late-Cretaceous thermal event of enigmatic geological position. *Contributions to Mineralogy and Petrology* **139**, 339–355.

Laurent V, Jolivet L, Roche V, Augier R, Scaillet S and Cardello GL (2016) Strain localization in a fossilized subduction channel: insights from the Cycladic Blueschist Unit (Syros, Greece). *Tectonophysics* **672**, 150–169.

Laurent V, Huet B, Labrousse L, Jolivet L, Monie P and Augier R (2017) Extraneous argon in high-pressure metamorphic rocks: distribution, origin and transport in the Cycladic Blueschist Unit (Greece). *Lithos* **272**, 315–335.

Laurent V, Scaillet S, Jolivet L, Augier R and Roche V (2021) ^{40}Ar behaviour and exhumation dynamics in a subduction channel from multi-scale ^{40}Ar/^{39}Ar systematics in phengite. *Geochimica et Cosmochimica Acta* **311**, 141–173.

Leake BE, Woolley AR, Arps CES, Birch WD, Gilbert MC, Grice JD, Hawthorne FC, Kato A, Kisch HJ, Krivovichev VG, Linthout K (1997) Nomenclature of amphiboles: report of the Subcommittee on Amphiboles of the International Mineralogical Association, commission on new minerals and mineral names. *European Journal of Mineralogy* **9**, 623–51.

Le Maitre RW (1976) Some problems of the projection of chemical data in mineralogical classifications. *Contributions to Mineralogy and Petrology* **56**, 181–189.

Lippolt HJ and Baranyi I (1976) Oberkretazische Biotit- und Gesteinsalter aus Kreta. *Neues Jahrbuch für Geologie und Paläontologie, Monatshefte* **7**, 405–414.

Maluski H, Bonneau M and Kienast JR (1987) Dating the metamorphic events in the Cycladic area: ^{39}Ar/^{40}Ar data from metamorphic rocks of the island of Syros (Greece). *Bulletin de la Société géologique de France* **3**, 833–842.

Manzotti P, Ballèvre M, Pitra P, Putlitz B, Robyr M and Müntener O (2020) The growth of sodic amphibole at the greenschist- To blueschist-facies transition (Dent Blanche, Western Alps): bulk-rock chemical control and thermodynamic modelling. *Journal of Petrology* **61**, egaa044.

Martha SO, Dörr W, Gerdes A, Petschick R, Schastok J, Xypolias P and Zulauf G (2016) New structural and U–Pb zircon data from Anafi crystalline basement (Cyclades, Greece): constraints on the evolution of a Late Cretaceous magmatic arc in the Internal Hellenides. *International Journal of Earth Sciences* **105**, 2031–2060.

Martha SO, Dörr W, Gerdes A, Krahl J, Linckens J and Zulauf G (2017) The tectonometamorphic and magmatic evolution of the Uppermost Unit in central Crete (Melambes area): constraints on a Late Cretaceous magmatic arc in the Internal Hellenides (Greece). *Gondwana Research* **48**, 50–71.

Martha SO, Zulauf G, Dörr W, Binck JJ, Nowara PM and Xypolias P (2019) The tectonometamorphic evolution of the Uppermost Unit south of the Dikti Mountains, Crete: *Geological Magazine* **156**, 1003–1026.

Mavrogonatos C, Magganas A, Kati M., Bröcker M and Voudouris, P (2021) Ophicalcites from the Upper Tectonic Unit on Tinos, Cyclades, Greece: mineralogical, geochemical and isotope evidence for their origin and evolution. *International Journal of Earth Sciences* **110**, 809–832.

McDonough WF and Sun S-S (1995) The composition of the Earth. *Chemical Geology* **120**, 223–253.

Melidonis NG (1980) The geological structure and mineral deposits of Tinos island (Cyclades, Greece). *The Geology of Greece* **13**, 1–80

Okrusch M and Bröcker M (1990) Eclogite facies rocks in the Cycladic blueschist belt, Greece: a review. *European Journal of Mineralogy* **2**, 451–478.

Paton C, Hellstrom J, Paul B, Woodhead J and Hergt J (2011) Iolite: freeware for the visualisation and processing of mass spectrometric data. *Journal of Analytical Atomic Spectrometry* **26**, 2508–2518.

Patzak M, Okrusch M and Kreuzer H (1994) The Akrotiri unit on the island of Tinos, Cyclades, Greece: witness to a lost terrane of Late Cretaceous age. *Neues Jahrbuch für Geologie und Paläontologie Abhandlungen* **194**, 211–252.

Pearce JA (1996) A user's guide to basalt discrimination diagrams. In *Trace Element Geochemistry of Volcanic Rocks: Applications for Massive Sulphide Exploration* (ed D.A. Wyman), Vol. **12**, 79–113. Geological Association of Canada, Short Course Notes.

Pearce JA, Harris NBW and Tindle AG (1984) Trace element discrimination diagrams for the tectonic interpretation of granitic rocks. *Journal of Petrology* **25**, 956–983.

Peillod A, Ring U, Glodny J and Skelton A (2017) An Eocene/Oligocene blueschist/greenschist-facies *P–T* loop from the Cycladic Blueschist Unit on Naxos Island, Greece: deformation-related reequilibration vs thermal relaxation. *Journal of Metamorphic Geology* **35**, 805–830.

Philippon M, Brun JP and Gueydan F (2011) Tectonics of the Syros blueschists (Cyclades, Greece): from subduction to Aegean extension. *Tectonics* **30**, TC4001.

Pe-Piper G and Photiades A (2006) Geochemical characteristics of the Cretaceous ophiolitic rocks of Ikaria Island, Greece. *Geological Magazine* **143**, 417–429.

Putlitz B, Cosca MA and Schumacher JC (2005) Prograde mica ^{40}Ar/^{39}Ar growth ages recorded in high pressure rocks (Syros, Cyclades, Greece). *Chemical Geology* **214**, 79–98.

Reinecke T, Altherr R, Hartung B, Hatzipangiotou K, Kreuzer H, Harre W, Klein H, Keller J, Geenen E and Boeger H (1982) Remnants of a Late-Cretaceous high-temperature belt on the island of Anafi (Cyclades, Greece). *Neues Jahrbuch für Geologie und Paläontologie, Abhandlungen* **145**, 157–182.

Ridley JR (1984) Listric normal faulting and the reconstruction of the synmetamorphic structural pile of the Cyclades. – In: Dixon, J.E. and Robertson, A.H.F. (eds.): The geological evolution of the eastern Mediterranean. *Geological Society, London, Special publication* **17**, 755–761.

Ring U, Thomson SN and Bröcker M (2003) Fast extension but little exhumation: the Vari detachment in the Cyclades, Greece. *Geological Magazine* **140**, 245–252.

Ring U, Glodny J, Will J and Thomson SN (2010) The Hellenic subduction system: high-pressure metamorphism, exhumation, normal faulting, and large-scale extension. *Annual Review of Earth and Planetary Sciences* **38**, 45–76.

Rollinson H and Pease V Using geochemical data (2021) *Using Geochemical Data to Understand Geological Processes*, pp 346. Cambridge University Press.

Ross PS and Bédard JH (2009) Magmatic affinity of modern and ancient subalkaline volcanic rocks determined from trace-element discriminant diagrams. *Canadian Journal of Earth Sciences* **46**, 823–839.

Sanchez-Gomez M, Avigad D and Heimann A (2002) Geochronology of clasts in allochthonous Miocene sedimentary sequences on Mykonos and Paros islands: implications for back-arc extension in the Aegean Sea. *Journal of the Geological Society* **159**, 45–60.

Seidel E, Okrusch M, Kreuzer H, Raschka H and Harre W (1976) Eo-Alpine metamorphism in the Uppermost Unit of the Cretan nappe system – petrology and geochronology. Part 1. The Léndas area (Asteroúsia Mountains). *Contributions to Mineralogy and Petrology* **57**, 259–275.

Seidel E, Okrusch M, Kreuzer H, Raschka H and Harre W (1981) Eo-Alpine metamorphism in the Uppermost Unit of the Cretan nappe system – petrology and geochronology. Part 2. Synopsis of high-temperature metamorphics and associated ophiolites. *Contributions to Mineralogy and Petrology* **76**, 351–361.

Soukis K and Stockli DF (2013) Structural and thermochronometric evidence for multi-stage exhumation of southern Syros, Cycladic Islands, Greece. *Tectonophysics* **595–596**, 148–164.

Tomaschek F, Baumann A, Villa IM, Kennedy A and Ballhaus C (2000a) Geochronological constraints on a Cretaceous metamorphic event from the Vari Unit (Syros, Cyclades, Greece). *Beihefte zum European Journal of Mineralogy* **12**, 214.

Tomaschek F, Kennedy A, Keay S and Ballhaus C (2000b) U/Pb-SHRIMP results for zircons from Syros, Greece: geochronological constraints on Carboniferous and Triassic magmatic episodes in the Cyclades. *Terra Nostra* 2000/5, 58.

Tomaschek F, Kennedy AK, Villa IM, Lagos M and Ballhaus C (2003) Zircons from Syros, Cyclades, Greece—Recrystallization and mobilization of zircon during high-pressure metamorphism. *Journal of Petrology* **44**, 1977–2002.

Uunk B, Brouwer F, de Paz-Álvarez M, van Zuilen K, Huybens R, van 't Veer R and Wijbrans J (2022) Consistent detachment of supracrustal rocks from a fixed subduction depth in the Cyclades. *Earth and Planetary Science Letters* **584**. doi: 10.1016/j.epsl.2022.117479

van Hinsbergen DJ, Peters K, Maffione M, Spakman W, Guilmette C, Thieulot C, Plümper O, Gürer D, Brouwer FM, Aldanmaz E and Kaymakcı N (2015) Dynamics of intraoceanic subduction initiation: 2. suprasubduction zone ophiolite formation and metamorphic sole exhumation in context of absolute plate motions, *Geochem Geophys Geosyst* **16**:1771–1785.

Verma SK and Armstrong-Altrin JS (2013) New multi-dimensional diagrams for tectonic discrimination of siliciclastic sediments and their application to Precambrian basins. *Chemical Geology* **355**, 117–133.

Verma SK, Pandarinath K and Verma SP (2012) Statistical evaluation of tectonomagmaticdiscrimination diagrams for granitic rocks and proposal of new discriminantfunction-based multi-dimensional diagrams for acid rocks. *International Geology Review* **54**, 325–347.

Vermeesch P (2006) Tectonic discrimination diagrams revisited. *Geochemistry, Geophysics, Geosystems* **7**. doi: 10.1029/2005GC001092.

Vermeesch P (2018) IsoplotR: a free and open toolbox for geochronology. *Geoscience Frontiers* **9**, 1479–93.

Wakabayashi J and Dilek Y (2000) Spatial and temporal relationships between ophiolites and their metamorphic soles: a test of models of forearc ophiolite genesis. *Geological Society of America Special Paper* **349**, 53–64.

Wakabayashi J and Dilek Y (2003) What constitutes "emplacement" of an ophiolite? Mechanisms and relationship to subduction initiation and formation of metamorphic soles. *Geological Society London, Special Publication* **218**, 427–447.

Wijbrans JR, Schliestedt M and York D (1990) Single grain argon laser probe dating of phengites from the blueschist to greenschist transition on Sifnos (Cyclades, Greece). *Contributions to Mineralogy and Petrology* **104**, 582–593.

Winchester J and Floyd P (1977) Geochemical discrimination of different magma series and their differentiation products using immobile elements. *Chemical Geology* **20**, 325–343.

Zeffren S, Avigad D, Heimann A and Gvirtzman Z (2005) Age resetting of hanging wall rocks above a low-angle detachment shear zone: Tinos Island (Aegean Sea). *Tectonophysics* **400**, 1–25.

Zulauf G, Linckens J, Beranoaguirre A, Gerdes A, Krahl J, Marschall HR, Millonig L-L, Neuwirth N, Petschick R, Xypolias P (2023) Long-term formation of barren skarn in a Triassic extensional setting: implications for the provenance of the Uppermost Unit of Crete, Greece. *International Journal of Earth Sciences* **112**, 1227–1250.

Zulauf G, Dörr W, Albert R, Martha SO and Xypolias P (2024) Provenance of far-traveled nappes in the eastern Mediterranean (Uppermost Unit, Crete): constraints from U–Pb zircon ages of detrital and igneous zircons. *International Journal of Earth Sciences* **113**, 23–47.

https://doi.org/10.1017/S0016756824000219 Published online by Cambridge University Press